CellPress

Neuron
Article

Lhx6 Directly Regulates *Arx* and *CXCR7* to Determine Cortical Interneuron Fate and Laminar Position

Daniel Vogt,[1,*] Robert F. Hunt,[2] Shyamali Mandal,[1,3] Magnus Sandberg,[1] Shanni N. Silberberg,[1] Takashi Nagasawa,[4] Zhengang Yang,[5] Scott C. Baraban,[2] and John L.R. Rubenstein[1,*]

[1]Department of Psychiatry, Neuroscience Program and the Nina Ireland Laboratory of Developmental Neurobiology, University of California San Francisco, San Francisco, CA 94158, USA

[2]Epilepsy Research Laboratory, Department of Neurological Surgery, University of California, San Francisco, San Francisco, CA 94143, USA

[3]Department of Cancer Biology and Pharmacology University of Illinois, Peoria, IL 61656, USA

[4]Department of Immunology and Hematology, Institute for Frontier Medical Sciences, Kyoto University, 53 Kawahara-cho, Shogoin, Sakyo-ku, Kyoto 606-8507, Japan

[5]Institutes of Brain Science, Fudan University, Shanghai 200032, China

*Correspondence: daniel.vogt@ucsf.edu (D.V.), john.rubenstein@ucsf.edu (J.L.R.)

http://dx.doi.org/10.1016/j.neuron.2014.02.030

SUMMARY

Cortical GABAergic interneurons have essential roles for information processing and their dysfunction is implicated in neuropsychiatric disorders. Transcriptional codes are elucidating mechanisms of interneuron specification in the MGE (a subcortical progenitor zone), which regulate their migration, integration, and function within cortical circuitry. Lhx6, a LIM-homeodomain transcription factor, is essential for specification of MGE-derived somatostatin and parvalbumin interneurons. Here, we demonstrate that some Lhx6$^{-/-}$ MGE cells acquire a CGE-like fate. Using an in vivo MGE complementation/transplantation assay, we show that Lhx6-regulated genes Arx and CXCR7 rescue divergent aspects of Lhx6$^{-/-}$ cell-fate and laminar mutant phenotypes and provide insight into a neonatal role for CXCR7 in MGE-derived interneuron lamination. Finally, Lhx6 directly binds in vivo to an Arx enhancer and to an intronic CXCR7 enhancer that remains active in mature interneurons. These data define the molecular identity of Lhx6 mutants and introduce technologies to test mechanisms in GABAergic interneuron differentiation.

INTRODUCTION

Disruptions in the balance of cortical excitation and inhibition are implicated in epilepsy, cognitive disorders, social dysfunction, and autism spectrum disorder (Chao et al., 2010; Cobos et al., 2005; Han et al., 2012; Rubenstein and Merzenich, 2003; Yizhar et al., 2011). In the forebrain most inhibition is generated by GABAergic interneurons, whereas glutamatergic projection neurons and thalamic afferents generate most cortical excitation. Multiple subgroups of GABAergic interneurons modulate distinct components of cortical circuits, in part through their physiological and molecular properties as well as their connectivity (Huang et al., 2007). In rodents, cortical interneurons arise from the subcortical medial and caudal ganglionic eminences (MGE and CGE, respectively) (Anderson et al., 1997; Wonders and Anderson, 2006), and the preoptic area (POA) (Gelman et al., 2011). The MGE gives rise to somatostatin (SST)$^+$ and parvalbumin (PV)$^+$ interneurons, while the CGE gives rise to vasoactive intestinal peptide (VIP)$^+$, serotonin receptor (5Ht3a)$^+$, Reelin$^+$;SST$^-$, and Sp8$^+$ interneurons (Cai et al., 2013; Kanatani et al., 2008; Lee et al., 2010; Ma et al., 2012; Rudy et al., 2011).

MGE identity is specified by the Nkx2-1 homeodomain transcription factor (TF), in part by inducing the expression of Lhx6 and Lhx8 LIM-homeodomain TFs (Sussel et al., 1999). Lhx6 and Lhx8 are coexpressed in the MGE subventricular zone (SVZ), where they have partially redundant functions (Flandin et al., 2011). Tangentially migrating and mature interneurons maintain Lhx6, but not Lhx8, expression (Grigoriou et al., 1998; Sussel et al., 1999). *Lhx6* mutants exhibit many phenotypes, including drastic reductions in SST$^+$ and PV$^+$ cortical interneurons, slowed tangential migration, and abnormal neocortical laminar position of interneurons. After tangential migration to the developing neocortex, MGE- and CGE-derived interneurons preferentially sort into deep and superficial layers, respectively, during neonatal ages (Miyoshi and Fishell, 2011). However, MGE-derived interneurons from *Lhx6* mutants fail to occupy middle neocortical layers and exhibit a preference for superficial and very deep layers (Liodis et al., 2007; Zhao et al., 2008). While Lhx6 promotes the expression of several genes that control cell fate and migration, including *Arx*, *Sox6*, *CXCR7* (Flandin et al., 2011; Zhao et al., 2008), and *Satb1* (Close et al., 2012; Denaxa et al., 2012), only the role of *Satb1* in the *Lhx6* phenotype has been evaluated.

We investigated the molecular and physiological phenotype of *Lhx6* mutant MGE cells and cortical interneurons. A subset of *Lhx6* mutant MGE cells exhibit molecular, functional, and laminar properties of CGE-like interneurons, particularly those in layer I that resemble the neurogliaform subgroup. To further characterize *Lhx6* mutant cells, we developed a

complementation/transplantation assay. Lentiviral-delivered genes are directed by cell-type-specific enhancers to MGE cells, allowing for the evaluation of in vivo phenotypes of transduced cells following transplantation into the neocortex. Restoration of *Arx* expression rescued the PV and SST phenotypes, while expression of CXCR7 partially rescued the lamination phenotype. We provide evidence that CXCR7 promotes the ability of transplanted interneurons to integrate into neocortical layer V. Finally, LHX6 directly binds enhancers near *Arx* and *CXCR7*, and this *CXCR7* enhancer drives expression in MGE-derived interneurons into postnatal stages.

RESULTS

Lhx6 Represses CGE-like Identity in MGE Cells

One hypothesis to explain the drastic loss of SST^+ and PV^+ interneurons and laminar deficits in *Lhx6* mutants (Liodis et al., 2007; Zhao et al., 2008) is that Lhx6 controls the regional fate of MGE cells. Thus, we tested whether $Lhx6^{PLAP/PLAP}$ mutant MGE cells expressed transcripts normally enriched in LGE- and/or CGE-derived cells: Sp8, COUPTFII (NR2F2), and 5HT3aR (Cai et al., 2013; Kanatani et al., 2008; Ma et al., 2012; Rudy et al., 2011), or the dorsal MGE marker cMaf (McKinsey et al., 2013). At E15.5, Sp8 was ectopically expressed in the MGE subventricular zone (SVZ) of *Lhx6* mutants (Figure 1A), but we did not observe changes in COUPTFII, 5HT3aR, and cMaf (Figures S1A–S1C available online). These results suggest a partial shift in molecular identity of mutant cells toward LGE/CGE fate. Similarly, in postnatal day (P) 14 or 17, brains of *Lhx6* mutants, 5HT3aR, COUPTFII, and c-Maf RNA expression were unaltered (Figures S1D–S1I and S1D′–S1I′), but numbers of $Sp8^+$ cells were increased in the neocortex at P17 (Figures 1B, 1F, 1K, and 1L: total $p = 0.02$, superficial II/III $p = 0.02$, deep $p = 0.02$).

Next, we assessed markers of CGE-derived (VIP) or CGE- and MGE-derived (CR and reelin) interneurons in P17 *Lhx6* mutants. The number and distribution of VIP^+ interneurons (Figures 1C, 1G, 1K, and 1M) was unchanged and CR^+ interneurons decreased ~3-fold (Figures 1D, 1H, 1K, and 1N: total $p = 0.0004$, superficial II/III $p = 0.0005$, deep $p = 0.003$). Reelin marks cortical interneurons in superficial neocortical layers (mostly CGE-derived) and deep layers (mostly MGE-derived) (Alcántara et al., 1998; Miyoshi et al., 2010). Total $reelin^+$ cells were reduced in *Lhx6* mutants (Figures 1E, 1I, and 1K: $p = 0.009$), especially in deep layers (Figure 1O: $p = 0.0002$). However, $reelin^+$ cells were significantly increased 1.3-fold in layer I (Figure 1O: superficial I $p = 0.02$). Together, these data show that *Lhx6* mutants exhibit an early and persistent increase in the number of interneurons expressing SP8, a CGE-derived interneuron marker, without any change in the number of VIP^+ interneurons. The concurrent decrease of reelin in deep layers, coupled with an increase in superficial layers ($reelin^{sup}$), is consistent with a loss of "MGE-type" interneurons and an increase in "CGE-type" interneurons.

Transplanted $Lhx6^{PLAP/PLAP}$ MGE-Derived Interneurons Exhibit Cell Autonomous Deficits in Cell Fate and Lamination

To test if known $Lhx6^{PLAP/PLAP}$ cortical phenotypes are cell autonomous and to further examine changes in molecular and laminar phenotypes, we used an MGE transplantation assay (Alvarez-Dolado et al., 2006; Cobos et al., 2005). E13.5 *CAG-dsRed* (Vintersten et al., 2004) MGE cells were transplanted into P1 wild-type (WT) neocortex and allowed to mature (Figure S2A). At 25 days posttransplant (DPT), similar numbers of control and $Lhx6^{PLAP/PLAP}$ transplanted $dsRed^+$ cells were detected in the neocortex (data not shown), and ~60% of control and mutant transplanted cells expressed the neuronal marker NeuN by this time point, (Figures S2B–2D). Very few *Lhx6* mutant transplanted cells expressed SST (Figure S3D: $p = 0.001$) and PV (Figure S2D: $p = 0.002$).

Next, we quantified the proportion of $dsRed^+$ cells residing in layer I, compared to all layers. The majority of control cells were distributed throughout layers II–VI with few at the lower border of layer I, whereas nearly half of the *Lhx6* mutant cells were found in layer I (Figure S2E: $p = 5.2 \times 10^{-7}$). Thus, transplanted $Lhx6^{PLAP/PLAP}$ cells recapitulate the cortical phenotypes found in the mutant mouse line, demonstrating that these defects are cell autonomous.

To further test the hypothesis of an MGE to CGE-like cell fate switch, we performed in vivo fate mapping studies using *Nkx2-1-Cre* (Xu et al., 2008) and the Cre-indicator line AI14, in which recombination activates expression of tdTomato (Madisen et al., 2010). $Nkx2\text{-}1\text{-}Cre;Lhx6^{PLAP/+}$ mice were crossed to $Lhx6^{PLAP/+};AI14$ mice, and we assessed for Sp8 and reelin in P13 $tdTomato^+$ neocortical cells. In controls, many $tdTomato^+$ cells were found in deep layers and did not express Sp8, however, ~13% of the $Lhx6^{PLAP/PLAP}$ $tdTomato^+$ cells expressed Sp8 ($p = 0.002$), ~22% of which were in layer I (Figures 2A–2F and 2N).

Next, we assessed the laminar position of $reelin^+$ cells that were in the *Nkx2-1*-lineage. Approximately 70% of the $reelin^+$ cells in deep layers (IV–VI) were $tdTomato^+$ (Figure 2M), indicating that the majority of these cells are MGE/POA-derived. $Lhx6^{PLAP/PLAP}$ brains had a decrease in the total number of $tdTomato^+/reelin^+$ cells (Figures 2K, 2L, and 2O, $p = 0.0008$). Furthermore, while controls had very few (<2%) of $tdTomato^+/reelin^+$ cells in layer I, ~45% of $Lhx6^{PLAP/PLAP}$ mutant cells were in layer I (Figure 2P, $p = 0.002$). Thus, we propose that a subset of $Lhx6^{PLAP/PLAP}$ MGE-derived interneurons acquire molecular and laminar properties resembling CGE-derived interneurons ($Sp8^+$ and $reelin^{sup}$).

$Lhx6^{PLAP/PLAP}$ MGE-Derived Interneurons Exhibit Late-Spiking Electrophysiological Properties

Lhx6 mutants are small and die before P18, prior to when the electrophysiology of interneurons can be reliably assessed. To circumvent this lethality and potential non-cell-autonomous effects, we generated a lentivirus, *Dlx1l2b-GFP*, to express genes specifically in forebrain GABAergic neurons (Arguello et al., 2013). Previous analyses showed that the *Dlx1l2b* enhancer is active in progenitors that generate the majority of forebrain GABAergic neurons (Ghanem et al., 2003; Potter et al., 2009). We transduced MGE cells with *Dlx1l2b-GFP* lentivirus, and then transplanted them into a WT host and allowed them to mature in vivo (Figure 3A). To test the efficiency of this approach, we transduced E13.5 *CAG-dsRed* MGE cells with *Dlx1l2b-GFP* lentivirus (Figure S3A), and then transplanted them into P1

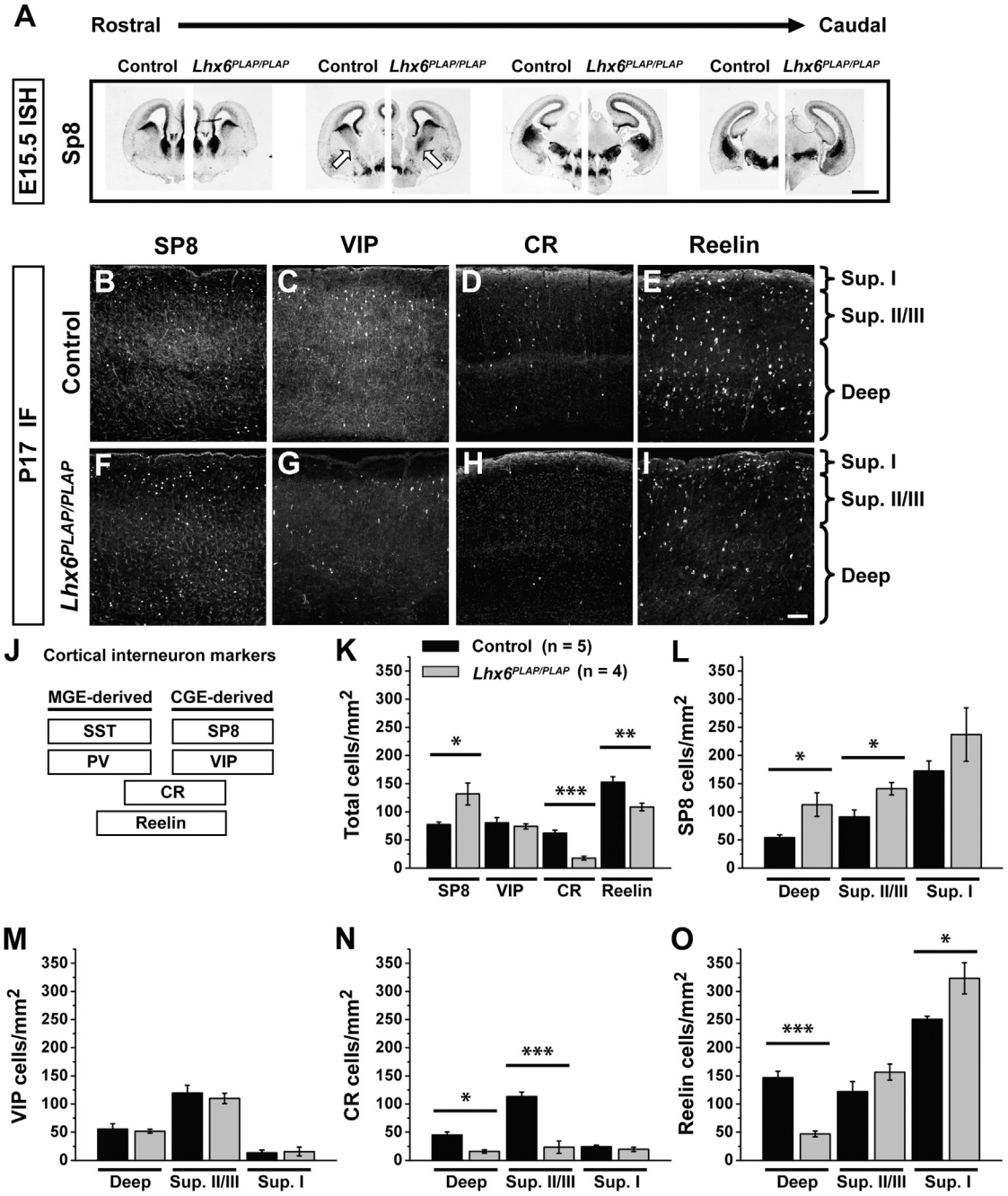

Figure 1. *Lhx6*$^{PLAP/PLAP}$ Progenitors and Interneurons Show a Partial Respecification of MGE-to-CGE Fate

(A) Rostral to caudal series showing in situ hybridization (ISH) for SP8 in control (left) and *Lhx6*$^{PLAP/PLAP}$ (right) E15.5 coronal hemisections. Arrows point to the MGE; the mutant has ectopic Sp8 expression. Scale bar represents 1 mm.

(B–I) Immunofluorescent (IF) images of CGE markers in the neocortex of control (B–E) and *Lhx6* mutant (F–I) coronal sections at P17. Scale bar in (I) represents 100 μm.

(J) Legend depicting relative distribution of molecular markers for MGE- and CGE-derived interneurons.

(K–O) Cell density quantification for VIP, CR, reelin, and Sp8. Cell density data shown for all layers (total) (K), superficial layers (sup. I and sup. II/III), and deep layers (deep) (L–O). Data are represented as mean ± SEM. One-way ANOVA was used to test significance among the groups: *$p < 0.05$, **$p < 0.01$, ***$p < 0.001$. See also Figure S1.

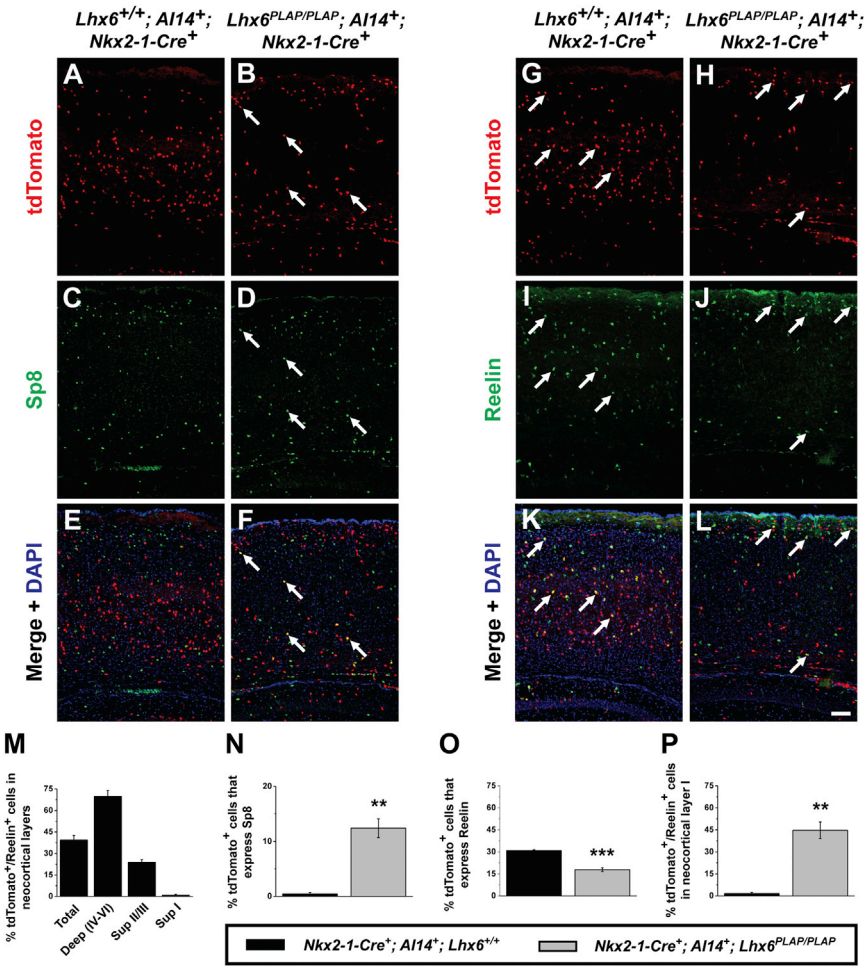

Figure 2. Fate Mapping of *Lhx6*$^{PLAP/PLAP}$ MGE-Derived Cells Reveals a Subset that Expresses CGE Markers

(A–L) Immunofluorescent images of P13 WT or *Lhx6*$^{PLAP/PLAP}$ neocortices from mice expressing *Nkx2-1-Cre* and the Cre-dependent tdTomato reporter (*Ai14*). MGE lineage cells (tdTomato$^+$) (A, B, G, and H) costained for Sp8 (C and D) or reelin (I and J). (E, F, K, and L) Merged images with DAPI (arrows point to examples of double-labeled cells). Scale bar in (L) represents 100 μm.

(M–P) Quantification of tdTomato$^+$/reelin$^+$ cells from WTs in neocortical layers. Quantification of the proportion of tdTomato$^+$ cells expressing Sp8 (N), reelin (O), and the proportion of tdTomato$^+$/reelin$^+$ cells in layer I (P). Data are represented as mean ± SEM. Student's t test was used to test significance among the groups: $^{**}p < 0.01$, $^{***}p < 0.001$.

See also Figure S2.

cortices. The *Dlx12b* enhancer is active throughout development and into adult stages. At 10 DPT, we found that ~50% of dsRed$^+$ cells were effectively transduced and expressed GFP (Figures S3C–S3E).

Next, we transplanted control and *Lhx6* mutant MGE cells transduced with *Dlx12b-GFP* lentivirus into P1 WT neocortex, and performed patch-clamp recordings of Dlx12b-GFP$^+$ cells in acute cortical slices at 35 DPT, (example cells, Figure 3B). Current injections into control and *Lhx6*$^{PLAP/PLAP}$ cells revealed four types of firing patterns: fast spiking, regular spiking, burst spiking, and late spiking (Figure 3C). All recorded neurons displayed electrophysiological properties consistent with functionally mature inhibitory neurons (Table S1), and both the passive membrane properties and active firing of each subgroup were comparable to previously described values (Miyoshi et al., 2010; Tricoire et al., 2011). Importantly, ~50% of the mutant cells (5/10) in layer I exhibited late-spiking properties (7/16, layers 1–3), whereas no control grafted cells had this property (0/18; all layers) (Figures 3D and 3D′). The layer I *Lhx6*$^{PLAP/PLAP}$ cells expressed GABA (data not shown). We also observed a few fast spiking neurons derived from *Lhx6* mutant cell grafts (3/25), suggesting that a few grafted mutant cells retain this property of MGE-derived interneurons.

Voltage-clamp recordings (−70 mV) detected spontaneous excitatory postsynaptic currents (EPSCs) in all control and mutant grafted interneurons (Figures 3C, 3E, and 3E′), consistent with their functional integration into the host neocortex. EPSCs were more frequent in fast spiking neurons compared to other subgroups (Table S1). In contrast, late-spiking neurons received low-frequency EPSCs that had relatively small amplitudes and fast rise-times (Table S1), features previously reported for late spiking neurogliaform cells (Chu et al., 2003; Armstrong et al., 2011) and layer I neurons (Zhou and Hablitz, 1997). However, for each interneuron subgroup identified on the basis of electrophysiological properties (e.g., fast spiking) we found no gross differences in the EPSC characteristics between mutants and controls (Table S1). Thus, *Lhx6* mutant MGE cells differentiated into physiologically mature GABAergic cortical interneurons that were functionally similar to controls, except that a large fraction of mutant interneurons exhibited late-spiking properties, a feature of neurogliaform interneurons (Miyoshi et al., 2010). Together, these electrophysiological, molecular (reelin and Sp8 expression), and laminar (neocortical layer I) properties indicate that many of the layer I *Lhx6* mutant MGE cells resemble neurogliaform interneurons.

Rescue of *Lhx6*$^{PLAP/PLAP}$ MGE Interneuron Fate via Transduction of Lhx6-Regulated Genes

Lhx6 is necessary for the expression of *Arx* and *Sox6* TFs and the *CXCR7* cytokine receptor (Batista-Brito et al., 2009; Flandin et al., 2011; Zhao et al., 2008). *Lhx8* MGE function is partially redundant for *Lhx6* (Flandin et al., 2011). To test if these factors were sufficient to complement specific *Lhx6* phenotypes, we developed an approach to transduce MGE cells before transplantation with a modified *Dlx12b-GFP* lentivirus that also

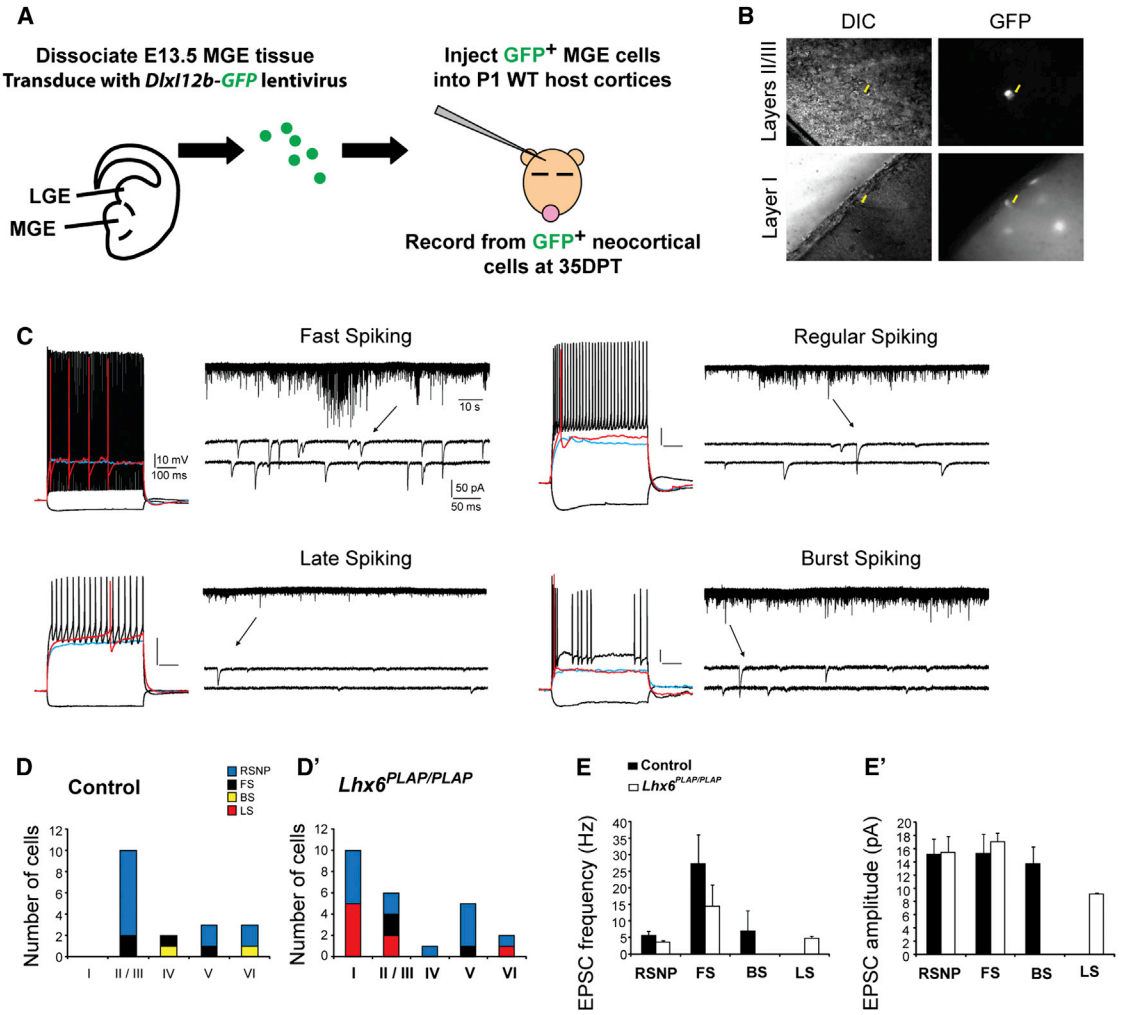

Figure 3. A Subset of *Lhx6*$^{PLAP/PLAP}$ MGE-Derived Interneurons Exhibit Late-Spiking Properties

(A) Schema: lentiviral transduction of E13.5 WT and *Lhx6* mutant MGE cells by a GABAergic-specific GFP reporter; cells are then transplanted into P1 WT neocortex to develop. GFP$^+$ cells are assessed at 35 DPT.

(B) Images of GFP$^+$ cells recorded from neocortical layers II/III and I (yellow arrows indicate recording pipette tip).

(C) Electrophysiological responses of four different transplanted MGE-GABAergic neurons: fast spiking (FS), regular spiking (RS), late spiking (LS), and burst spiking (BS). Current-clamp traces (left side) following a hyperpolarizing current pulse (−50 pA; black) and depolarizing pulses at subthreshold (blue), near threshold (red), and near maximal firing (black). Shown on right: 2 min voltage-clamp recordings of sEPSCs for each cell. A region of each trace is expanded below (arrows) to show event waveforms.

(D and D′) Histograms summarizing the subgroups of recorded neurons in each layer.

(E and E′) Mean sEPSC frequency and amplitude for each interneuron subgroup. Data are represented as mean ± SEM.

See also Figure S3 and Table S1.

encoded these genes (Figure 4A, schema). The genes were inserted downstream of a T2a element in the viral vector (Figure S3A), and the expression of each protein was confirmed (Figure S3B).

E13.5 MGE cells (control or *Lhx6*$^{PLAP/PLAP}$) were transduced with *Dlxi12b-GFP*, transplanted, and assessed at 35 DPT. GFP$^+$ control transplants expressed SST (~50%) and PV (~23%) at expected frequencies (Figures 4B, 4H, 4N, and 4O). GFP-transduced *Lhx6*$^{PLAP/PLAP}$ transplants had a drastic reduction in SST$^+$ (~2%) and PV$^+$ (~3%) interneurons (Figures 4B′, 4H′, 4N′, and 4O′), recapitulating the *Lhx6*$^{PLAP/PLAP}$ phenotypes.

Lhx6 transduction into *Lhx6* mutant MGE cells rescued SST and PV expression to approximately WT levels (Figures 4C′, 4I′, 4N′, and 4O′: SST $p = 4.01 \times 10^{-10}$, PV $p = 0.0002$). Thus, despite a delayed onset of expression (*Lhx6* expression is initiated in WT mice at ~E10.5), rescued cells still differentiate with properties of MGE-derived interneurons. Moreover, like *Lhx6*, *Lhx8* transduction of *Lhx6* mutant MGE cells rescued PV (Figures 4J′ and 4O′: $p = 0.0002$), and mostly rescued SST (Figures 4D′ and 4N″: $p = 1.88 \times 10^{-7}$). *Lhx8* promotes development of telencephalic choline acetyltransferase (ChAT) neurons (Zhao et al., 2003; Fragkouli et al., 2009). However, expression

of *Lhx8* did not induce ectopic ChAT expression in transplanted MGE cells (Figures S4A–S4G). On the other hand, *Lhx8* transduction restored SOX6 expression in the *Lhx6* mutant cells (Figures S4H–S4O), providing further evidence for its redundancy with *Lhx6*.

Arx and *Sox6* expression in *Lhx6* mutant MGE appears normal, but is not maintained in tangentially migrating MGE cells (Zhao et al., 2008). *Sox6* transduction rescued neither SST (Figures 4F′ and 4N′) nor PV expression (Figures 4L′ and 4O′). In contrast, *Arx* transduction of *Lhx6* mutant MGE cells restored ~25% of the SST cells (Figures 4E′ and 4N′: p = 0.01) and ~80% of the PV cells (Figures 4K′ and 4O′: p = 0.002). Denaxa et al. (2012) found that *Satb1* is downstream of *Lhx6* and promotes SST expression. We also detected loss of Satb1 expression in *Lhx6* mutants (Figures S5A–S5F) but *Arx* transduction did not rescue Satb1 expression in *Lhx6* mutants (Figures S5G–S5L).

CXCR7 expression in the *Lhx6* mutants is greatly reduced in the MGE and tangentially migrating MGE cells (Zhao et al., 2008). Transduction of CXCR7 into *Lhx6* mutant MGE cells rescued neither SST (Figures 4G′ and 4N′) nor PV (Figures 4M′ and 4O′) expression, but did partially rescue the lamination phenotype (see next section).

Transducing *Lhx6*, *Lhx8*, or *Arx* into control MGE cells did not significantly change the numbers of interneuron subgroups (Figures 4C–4E, 4I–4K, 4N, and 4O). However, transduction of *Sox6* and *CXCR7* altered the numbers of SST$^+$ and PV$^+$ interneurons. *Sox6* increased SST$^+$ cells (Figure 4N: p = 0.04) and concurrently promoted a trend for decreased PV$^+$ cells (Figure 4O). This effect was more pronounced in *Lhx6*$^{+/+}$ cells (SST p = 0.0002, PV p = 0.01) than *Lhx6*$^{PLAP/+}$ cells (SST p = 0.008, PV p = n.s.) (data not shown). Of note, control MGE cells transduced with *CXCR7* generated normal numbers of SST$^+$ cells (Figures 4G and 4N), but ~50% reduction of PV$^+$ cells (Figures 4M and 4O: p = 0.005).

Together, these data show that while *Lhx6*, *Lhx8*, and *Arx* were sufficient to rescue *Lhx6*$^{PLAP/PLAP}$ SST and PV phenotypes, *Sox6* did not rescue these deficits. However, gain-of-function assays suggest *CXCR7* and *Sox6* dosage may regulate the SST/PV ratio, the latter is consistent with *Sox6* loss-of-function data (Azim et al., 2009; Batista-Brito et al., 2009).

Lamination Defects of *Lhx6*$^{PLAP/PLAP}$ Interneurons Are Rescued by *Lhx6*, *Lhx8*, and *CXCR7*

Lhx6 mutant interneurons have abnormal laminar positions in the postnatal neocortex, mostly occupying superficial and very deep layers (Liodis et al., 2007; Zhao et al., 2008). We found that this laminar phenotype is cell autonomous, as many transplanted E13.5 *Lhx6* mutant interneurons occupy superficial layers (Figure S2). We next asked if *Lhx6*, or its downstream factors, could rescue the laminar phenotype (layer I localization) of *Lhx6* mutant cells, by assessing the proportion of transplanted cells in layer I at 35 DPT transduced with *GFP*-, *Lhx6*-, or *Lhx6*-regulated factors.

Control MGE cells, transduced with *GFP*-, *Lhx6*-, or *Lhx6*-regulated factors, rarely (~10%) were found in neocortical layer I (Figure 5A), with the majority at the I/II border. By contrast, half of the *GFP*-transduced, *Lhx6* mutant MGE cells occupied layer I (Figure 5B). Transduction of *Lhx6* or *Lhx8* decreased mutant cells found in layer I to control levels (Figure 5B: Lhx6, p = 0.002; Lhx8 p = 0.0005). Transduction of *Arx* or *Sox6* did not rescue the laminar distribution (Figure 5B). However, transduction of *CXCR7* induced an ~2-fold reduction of cells in layer I (Figure 5B: p = 0.01), suggesting that reduced levels of *CXCR7* contributes to the *Lhx6*$^{PLAP/PLAP}$ laminar phenotype.

Lhx6 Transduction Partially Rescues *Lhx6*$^{PLAP/PLAP}$ CGE-like Characteristics

Transduction of *Arx* and *CXCR7* rescued divergent aspects of the *Lhx6* mutant phenotypes, perhaps via suppression of CGE-like molecular phenotypes. Thus, we first assessed reelin expression in transduced MGE transplants at 35 DPT (Figures 5C–5J). GFP transduction recapitulated the previous phenotypes (Figures 1 and 2), with *Lhx6* mutants exhibiting ~30% reduction in reelin$^+$ cells (Figures 5C, 5G, 5K, and 5K′) and ~60% in neocortical layer I (Figure 5L′). Transduction of *Lhx6* into *Lhx6*$^{PLAP/PLAP}$ MGE cells increased the total number of reelin$^+$ cells (Figures 5H and 5K′: p = 0.009) and reduced reelin$^+$ cells in layer I ~20-fold (Figure 5L′: p = 0.0001). *CXCR7* transduction induced an ~2-fold reduction of reelin$^+$ cells in layer I (Figure 5L′: p = 0.005). Transduced control cells did not show changes in reelin$^+$ cell numbers (Figure 5K), although reelin$^+$ cells in layer I were reduced by *Lhx6* and *Arx* transduction (Figure 5L: Lhx6 p = 0.002; Arx p = 0.02). Despite changes in reelin, ectopic Sp8 was still observed in transplanted *Lhx6* mutant MGE cells transduced with either *Lhx6, Arx, CXCR7 or GFP* (Figure S6 and data not shown), suggesting that a full reversal of CGE properties did not occur. Despite the inability of *Lhx6* to reverse the ectopic expression of Sp8, *Lhx6* transduction increased the total number of reelin$^+$ interneurons, and decreased reelin$^+$ interneurons in layer I (Figures 5K′ and 5L′). Moreover, while *Arx* and *CXCR7* were sufficient to restore MGE molecular and laminar properties in the *Lhx6* mutants, neither were able to rescue the reelin phenotype as completely as *Lhx6*, suggesting that additional *Lhx6*-regulated factor(s) contribute to this process.

Transplanted MGE Cells Lacking CXCR7 or CXCR4 Exhibit Deficits in Integration into Neocortical Layer V

The ability of *CXCR7* to rescue the laminar position of *Lhx6*$^{PLAP/PLAP}$ interneurons (Figure 5B) prompted us to ask if *CXCR7* influenced transplanted MGE cell integration into deep neocortical layers. The chemokine CXCL12 is the principal ligand for CXCR7; its prenatal expression in the cortical meninges and intermediate zone attracts immature cortical interneurons expressing CXCR4 and CXCR7, promoting their tangential migration along superficial and deep pathways, and preventing their premature entry into the cortical plate (Sánchez-Alcañiz et al., 2011; Stumm et al., 2003; Wang et al., 2011). Later, CXCL12 mRNA is present in deep cortical layers in the neonatal brain (Schönemeier et al., 2008; Stumm et al., 2003), and GFP expression from the CXCL12 locus (Ara et al., 2003) reveals postnatal expression in neocortical layer V pyramidal neurons (Figures S7A–S7C). We hypothesized that postnatal expression of CXCL12 may influence the laminar distribution of transplanted MGE cells by attracting some transplanted MGE cells into neocortical layer V. Toward assessing this, we investigated the laminar position of transplanted MGE cells lacking

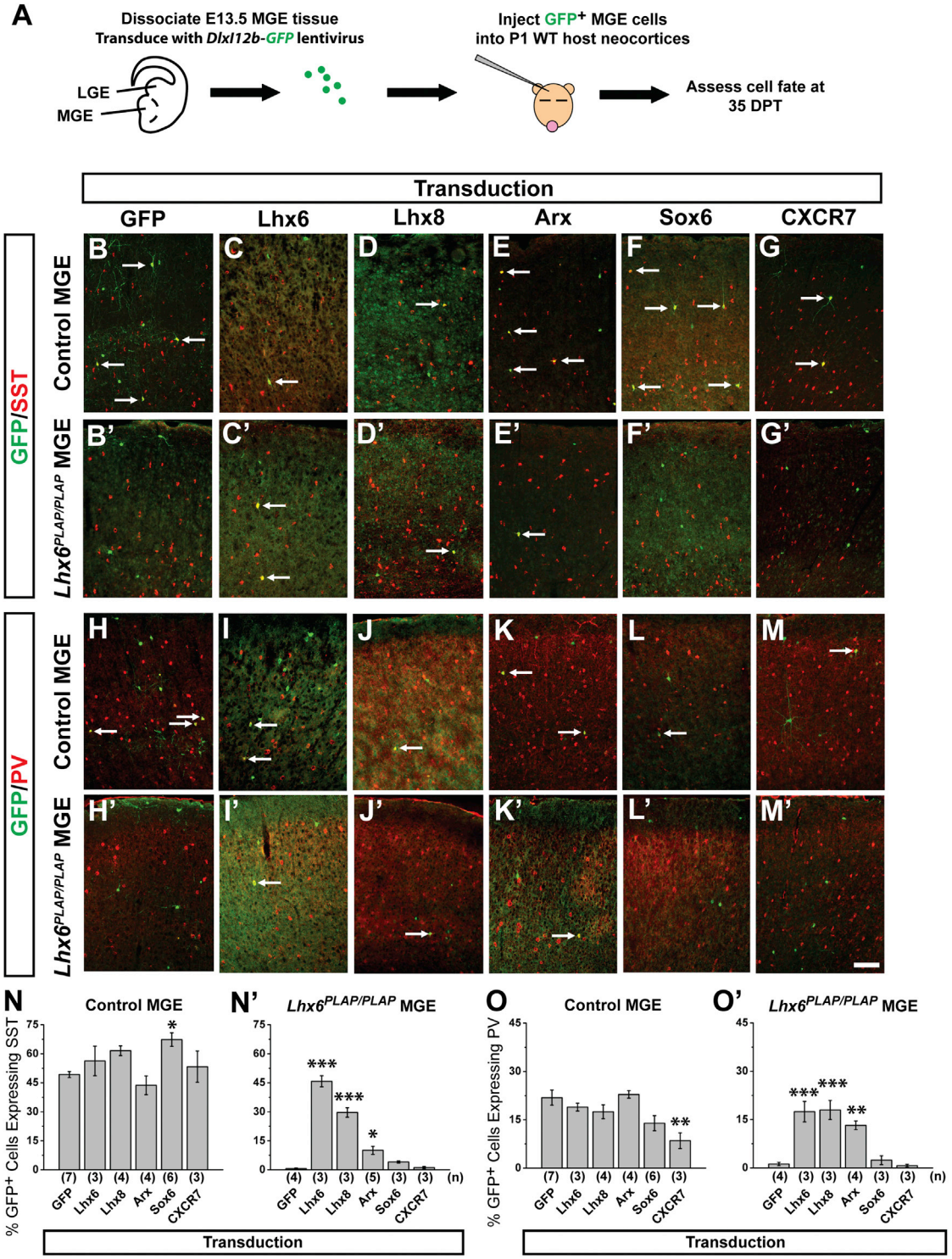

Figure 4. Rescue of *Lhx6*$^{PLAP/PLAP}$ Cell Fate Phenotypes via Transduction of Lhx6, Lhx8, and Arx

(A) Schema: E13.5 WT and mutant MGE cells are transduced with viruses expressing coding regions for *GFP*, *Lhx6*, *Lhx8*, *Arx*, *Sox6*, or *CXCR7,* and transplanted into P1 WT hosts. GFP$^+$ cells are assessed at 35 DPT for SST or PV expression.

(B–M′) Immunofluorescence showing merged staining of GFP (green) with SST or PV (red) in the neocortex of controls (B–M) and *Lhx6*$^{PLAP/PLAP}$ (B′–M′). Scale bar in (M′) represents 100 μm.

(N and N′) Proportion of GFP$^+$ cells that express SST for control (N) and *Lhx6*$^{PLAP/PLAP}$ (N′) transplants.

(legend continued on next page)

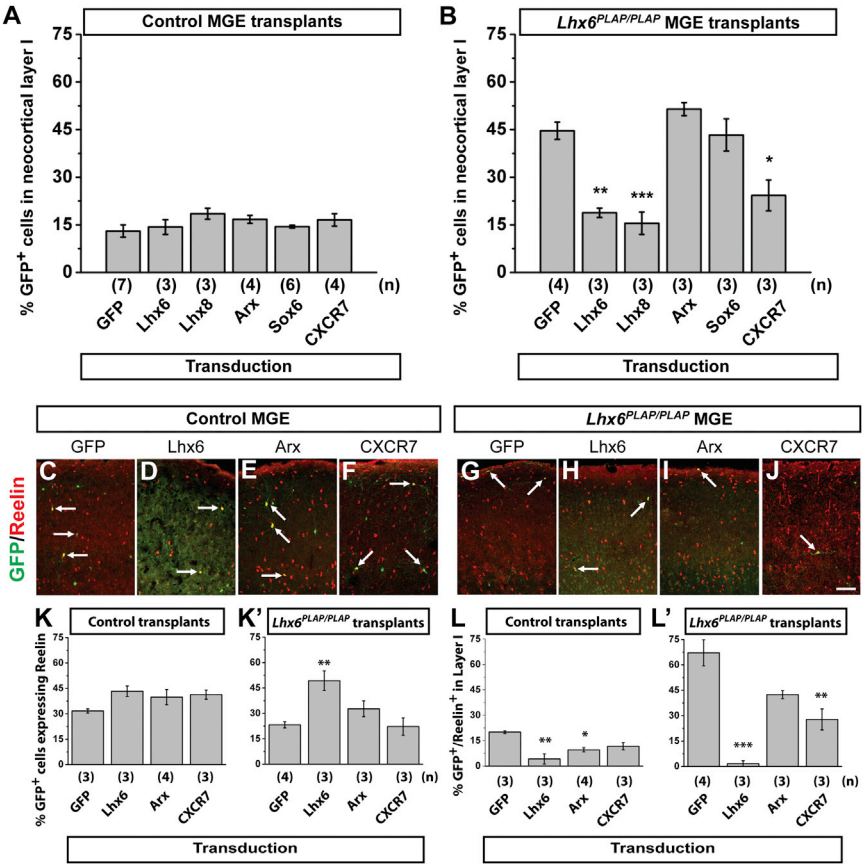

Figure 5. Rescue of *Lhx6*$^{PLAP/PLAP}$ Lamination Deficits via Transduction of Lhx6, Lhx8, and CXCR7

Proportion of transduced cells at 35 DPT that occupy neocortical layer I for control (A) and *Lhx6*$^{PLAP/PLAP}$ (B) MGE transplants. Two color immunofluorescence showing merged staining for GFP (green) and reelin (red) in the neocortex at 35 DPT of control (C–F) or *Lhx6*$^{PLAP/PLAP}$ (G–J) transplants. Arrows point to double-labeled cells. Quantification of GFP$^+$/reelin$^+$ transplanted control (K) and *Lhx6*$^{PLAP/PLAP}$ (K′) cells. Quantification of transplanted GFP$^+$/reelin$^+$ control (L) or *Lhx6*$^{PLAP/PLAP}$ (L′) cells in layer I. Data are represented as mean ± SEM. One-way ANOVA was used to test significance among the groups: *$p < 0.05$, **$p < 0.01$, ***$p < 0.001$ compared to GFP transduction alone. Scale bar in (J) represents 100 μm.

See also Figure S6.

either *CXCR7* or *CXCR4* at two time points: 7 DPT, when cells are still migrating; 30 DPT, when cells are nearly mature.

First, E13.5 *CAG-dsRed*$^+$ (controls), or *CAG-dsRed*$^+$*; CXCR7*$^{-/-}$ (Sierro et al., 2007) MGE cells were transplanted into P1 *CXCL12-GFP* neocortices and laminar position was assessed at 7 DPT (Figure 6A, schema). Because *CXCR7* mutants have little to no CXCR4 protein (Sánchez-Alcañiz et al., 2011), the mutant interneurons should lose their ability to respond to CXCL12. At 7 DPT, the *CXCR7*$^{-/-}$ interneurons accumulated in superficial layers and were reduced in layer V (Figures 6B–6D, $p < 0.001$).

To test if *CXCR7*$^{-/-}$ interneuron laminar deficits persist in the adult cortex, and to explore whether CXCR4 and CXCR7 have different functions, we transplanted E13.5 *Lhx6-GFP*$^+$ MGE cells from control, *CXCR4*$^{-/-}$ or *CXCR7*$^{-/-}$ embryos (Figure 6E). Analysis at 30 DPT revealed that *CXCR4*$^{-/-}$ and *CXCR7*$^{-/-}$ MGE interneurons accumulated in superficial layers and were reduced in layer V (Figures 6F–6I: *CXCR4*$^{-/-}$ and *CXCR7*$^{-/-}$ compared to controls $p < 0.05$). Together, the 7 and 30 DPT data suggest that CXCR4/7-signaling in the neonatal cortex regulates the targeting of some interneurons to layer V.

Because *CXCR7* transduction into WT MGE cells decreased PV$^+$ numbers (Figure 4O), we tested whether loss of *CXCR7* influenced the PV/SST ratio using the MGE transplantation assay. *CXCR7*$^{-/-}$ transplants exhibited a 50% reduction in PV$^+$ cells compared to controls (Figures 6M, 6O, and 6Q: $p = 0.006$). However, *CXCR4*$^{-/-}$ transplants did not exhibit a significant decrease in PV (Figures 6N and 6Q). There were no gross changes in SST levels among groups (Figures 6J–6L and 6P). Thus, in addition to promoting MGE-derived interneuron migration, imbalances in CXCR7 levels, but not CXCR4, may regulate PV interneuron differentiation or maturation.

Lhx6 Directly Binds and Activates *Arx* and *CXCR7* Enhancers

We next asked if *Lhx6* could directly regulate *Arx* and *CXCR7* by screening potential enhancers near their genomic loci (Figure 7A). Enhancers near *Arx* have been identified that are active during telencephalon development (Colasante et al., 2008). An *Arx* enhancer region within the *PolA1* locus drives expression in developing basal ganglia, while regions closer to *Arx* drive expression in embryonic neocortex. We screened the basal ganglia *Arx* enhancer and regions near the *CXCR7* locus using MatInspector to predict sites containing putative Lim-homeodomain binding sites. The *Arx* enhancer contained five sites, (A1–A5), (Figure 7A, top), and several sites were found near *CXCR7*, (C1–C10), including seven in the intron (Figure 7A, bottom).

To test if these sites (Figure 7A, black bars) were bound by Lhx6 in vivo, we generated an antibody against Lhx6 and

(O and O′) Proportion of GFP$^+$ cells that express PV for control (O) and *Lhx6*$^{PLAP/PLAP}$ (O′) transplants. Data are represented as mean ± SEM. One-way ANOVA was used to test significance among the groups: *$p < 0.05$, **$p < 0.01$, ***$p < 0.001$ compared to GFP transduction alone. Arrows point to GFP$^+$ cells that coexpress the indicated marker.

See also Figures S3–S5.

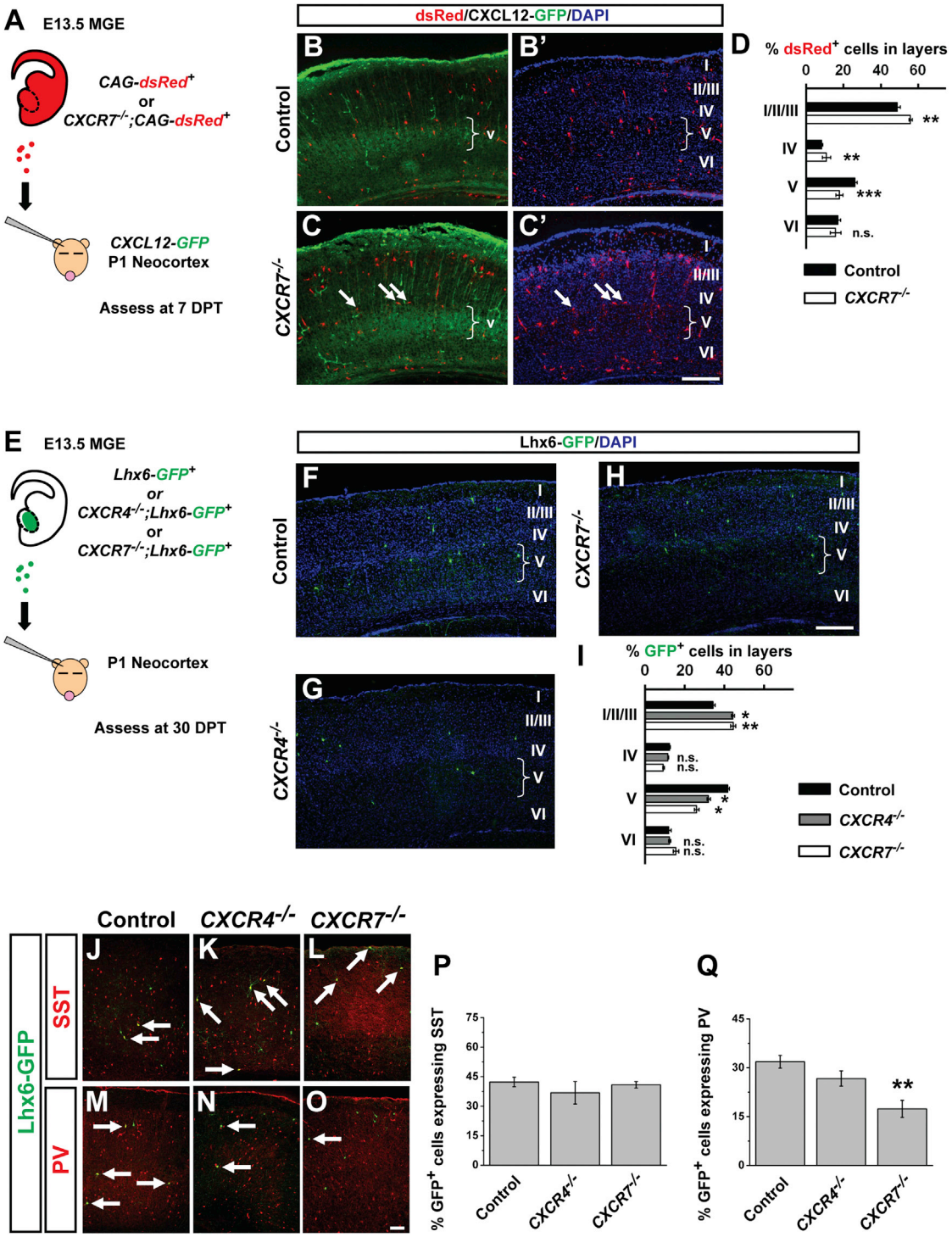

Figure 6. *CXCR7* and *CXCR4* Regulate Laminar Position of Transplanted MGE Cells

(A) Schema depicting transplant of E13.5 *CAG-dsRed*$^+$ MGE cells into P1 *CXCL12-GFP* reporter hosts.

(B–C′) Immunofluorescent images of transplanted MGE cells in the neocortex at 7 DPT, arrows in (C) and (C′) point to dsRed$^+$ cells at the IV/V border that lie outside of the CXCL12-GFP$^+$ domain in layer V. Brackets show the width of layer V. Scale bar in (C′) represents 250 μm.

(D) Quantification of *CAG-dsRed*$^+$ cells in neocortical layers at 7 DPT.

(E) Schema depicting transplant of E13.5 *Lhx6-GFP*$^+$ MGE cells into P1 WT hosts.

(legend continued on next page)

performed chromatin immunoprecipitation from E13.5 MGEs. *Arx* site A3 showed enrichment over input (Figure 7B: p = 0.03), as did sites A2, A4, and A5, whereas site A1 did not show Lhx6 binding (Figure 7B and data not shown). Site C8 in the *CXCR7* intron was also bound by Lhx6 (Figure 7B: p = 0.007).

We then tested if Lhx6 and its cofactor Ldb1 could modulate expression from the candidate *CXCR7* intronic enhancer (Figure 7A, red bar). Driving Lhx6/Ldb1 expression in P19 cells led to ~4-fold increase in activity of a luciferase reporter plasmid containing the *CXCR7* intron (PGL4.23-*CXCR7-int*), compared to a control (PGL4.23) plasmid lacking the *CXCR7* intron (Figure 7C: p = 0.01).

Finally, we tested the activity of the *CXCR7* intron enhancer in slice culture and in vivo. We inserted the *CXCR7* intron upstream of *GFP*, and in a separate vector we inserted the GABAergic enhancer, *Dlx56i* (Zerucha et al., 2000), upstream of mCherry. We then coelectroporated them into E13.5 tissue slices containing LGE, MGE, and CGE (Figure S8A). While mCherry was detected in the LGE, MGE, and CGE, GFP expression was largely restrict to the MGE (Figures S8B, S8B″, S8D, and S8D″). Moreover, many mCherry$^+$ cells migrating out of the MGE expressed GFP, suggesting that the *CXCR7* intron is active in MGE-derived GABAergic interneurons. To test this idea, we examined whether the *CXCR7* intron could drive expression in MGE-derived SST$^+$ and PV$^+$ interneurons. E13.5 *AI14*$^+$ MGE cells were transduced with a *CXCR7* intron-*GFP*-T2a-*Cre* lentivirus (Figure 7D), transplanted into a P1 WT host and assessed at 35 DPT. At 35 DPT, ~60% of the GFP$^+$ cells expressed SST and ~20% expressed PV (Figure 7D). Fate mapped tdTomato$^+$ cells marked similar proportions of SST$^+$ and PV$^+$ cells. Furthermore, by dividing the number of GFP$^+$ cells by the number of tdTomato$^+$ cells, we determined that ~50% of the transduced cells maintained enhancer activity by 35 DPT.

Overall, these data show that Lhx6 directly bound to enhancer elements near *Arx* and *CXCR7,* where it may promote expression of these genes. Furthermore, the newly discovered *CXCR7* intronic enhancer was highly expressed in the MGE, and in mature SST$^+$ and PV$^+$ interneurons.

DISCUSSION

Lhx6 mutants have defects in MGE-derived cortical interneuron development, including loss of PV$^+$ and SST$^+$ interneurons and a preference to occupy both superficial and very deep neocortical layers (Liodis et al., 2007; Zhao et al., 2008). Previous molecular analyses identified downregulated genes in *Lhx6* mutants that may contribute to these phenotypes, including *Arx*, *CXCR7*, *Satb1*, and *Sox6* (Close et al., 2012; Denaxa et al., 2012; Flandin et al., 2011; Zhao et al., 2008). Here, we report aspects of the *Lhx6* molecular phenotype and its downstream genes (Figure 7E, schema). A subset of *Lhx6* mutant MGE-derived cells exhibit molecular and laminar properties of CGE-derived interneurons. Moreover, the reelin$^+$ cells in neocortical layer I have properties of neurogliaform interneurons (Miyoshi et al., 2010). Finally, we developed a complementation assay to demonstrate that specific aspects of the *Lhx6* mutant phenotype are rescued by *Arx* and *CXCR7*, revealing functions of these genes in interneuron development.

Lhx6 Represses CGE Interneuron Fate

The rostrodorsal MGE is a major source of PV$^+$ and SST$^+$ cortical interneurons (Flandin et al., 2010; Rudy et al., 2011). In *Lhx6* mutants, this progenitor zone maintains many of its normal properties, perhaps because the MGE cells still express *cMaf*, *Lhx8*, *Nkx2-1*, and *Sox6* (Flandin et al., 2011; Zhao et al., 2008) (Figure S1). However, in *Lhx6* mutants the rostrodorsal MGE ectopically expressed *Sp8* (Figure 1); *Sp8* ordinarily marks the CGE and LGE, but not the MGE or POA (Ma et al., 2012). These results suggest that *Lhx6* functions not only in the maturation of MGE-derived neurons, but is also required for fate specification of SVZ cells in the rostrodorsal MGE. This is due, in part, to repression of molecular characteristics of CGE-derived progenitors (*Sp8*) and interneurons (Sp8, reelin$^+$;SST$^-$) (Figures 1 and 2). Moreover, these fate changes are likely cell autonomous, because *Lhx6* mutant MGE cells exhibited similar changes in Sp8 and reelin expression (Figures 5 and S6). A partial fate change may explain why a subset of *Lhx6* mutant cortical interneurons occupy neocortical layer I. While *Lhx6* mutant interneurons in layer I resemble neurogliaform cells, this cell type is not exclusively derived from the CGE, as some come from the MGE (Tricoire et al., 2010). However, we are unaware of MGE-derived interneurons that occupy layer I. Despite these CGE-like properties, *Lhx6* mutant MGE cells did not express other markers of CGE-derived interneuron subgroups, such as 5HT3aR and VIP (Figures 1 and S1) (Lee et al., 2010; Miyoshi et al., 2010), suggesting that these changes in cell fate and laminar position are partial. Overall, these data reveal a role for Lhx6 in mediating MGE interneuron identity and offer insights into the mechanisms underlying *Lhx6* mutant phenotypes.

Arx Functions Downstream of *Lhx6* in Promoting PV and SST Expression

To study the individual functions of genes with reduced expression in *Lhx6* mutants, we developed an MGE complementation assay using lentiviral technology and a cell-type-specific enhancer to rescue phenotypic changes of a specific mutant. We defined rescue as the ability of a transduced factor to restore, or complement, a phenotypic change in mutant cells to control levels. The *Dlx12b* enhancer (Ghanem et al., 2003) can be used in lentiviral vectors to drive gene expression in MGE cells,

(F–H) Lhx6-GFP immunofluorescence (green) merged with DAPI (blue) in neocortex of mice in which either Control, *CXCR4*$^{-/-}$ or *CXCR7*$^{-/-}$ E13.5 *Lhx6-GFP*$^+$ MGE cells were transplanted into P1 WT neocortex and assessed at 30 DPT. Scale bar in (H) represents 250 μm.
(I) Proportion of GFP$^+$ Cells in Neocortical Layers of WT *CXCR4*$^{-/-}$ and *CXCR7*$^{-/-}$ MGE Cells
(J–Q) Immunofluorescence of 30 DPT transplants stained for SST (J–L) or PV (M–O), arrows point to coexpressing cells. Quantification of the proportion of Lhx6-GFP+ MGE cells that express SST (P) or PV (Q). Data are represented as mean ± SEM. Chi-square test (for lamination) or one-way ANOVA (for cell fate proportion) was used to test significance between groups. *p < 0.05, **p < 0.01, ***p < 0.001. Scale bar in (O) represents 100 μm.
See also Figure S7.

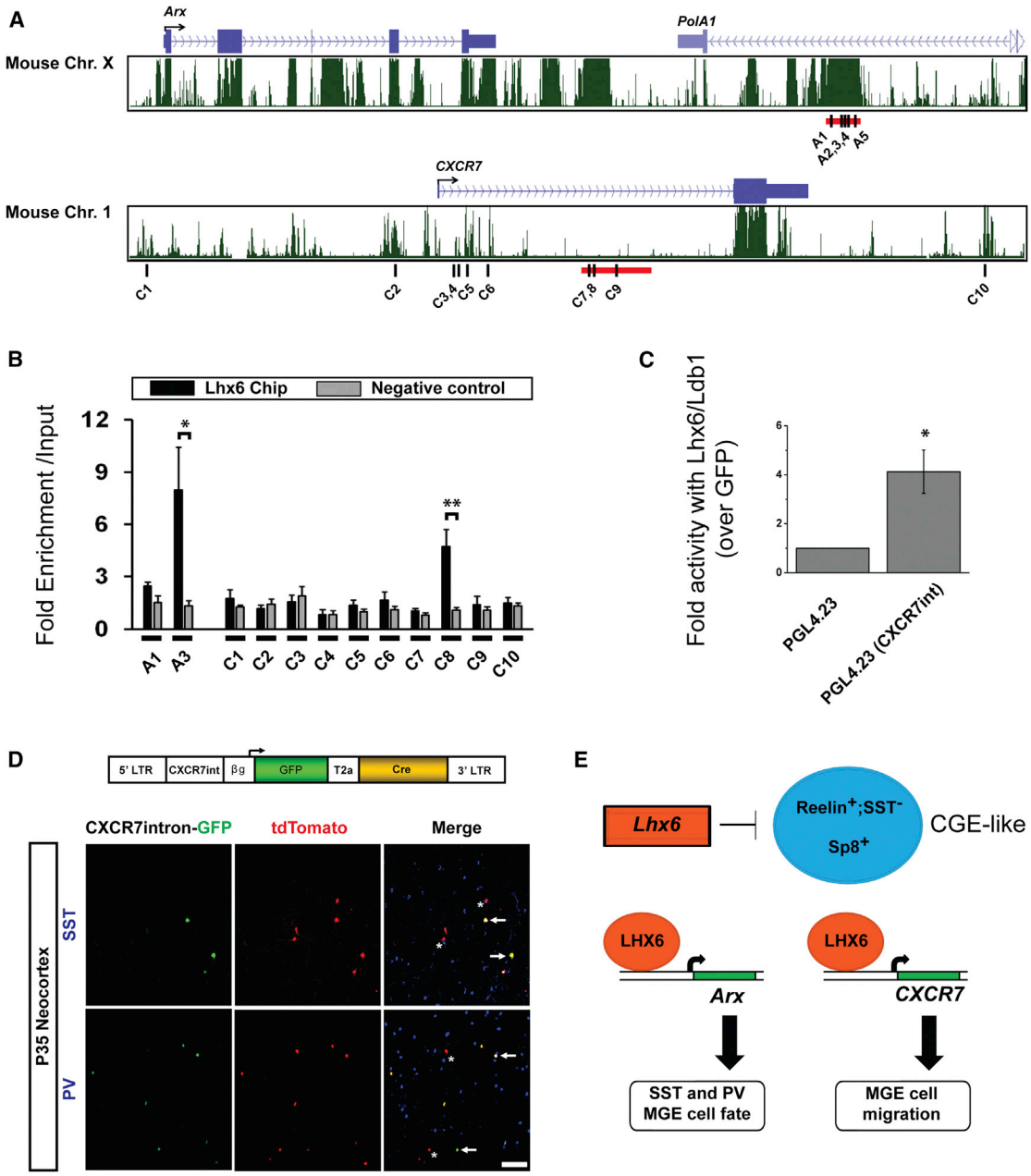

Figure 7. Lhx6 Directly Binds *Arx* and *CXCR7* Enhancers, and the *CXCR7* Enhancer Is Active in MGE Interneurons

(A) Genomic regions near *Arx* (top, MM9: 90,530,800-90,562,350) and *CXCR7* (bottom, MM9: 92,090,350-92,120,000) loci from University of California, Santa Cruz (UCSC) genome browser.

(B) LHX6 ChIP-qPCR assay for regions in the *Arx* enhancer (A1, 3), and the *CXCR7* locus (C1–10).

(C) Luciferase assay from P19 cells, transfected either with a *GFP* expression vector or *Lhx6-GFP* and *Ldb1* vectors in the presence of either a luciferase vector lacking an enhancer (PGL4.23) or a luciferase vector with the *CXCR7-intron* enhancer.

(D) *AI14*$^{+}$ E13.5 MGE cells were transduced with a *CXCR7-intron-GFP-T2a-Cre* lentivirus (top) and transplanted into a WT P1 cortex. Immunofluorescence shows expression of 35 DPT coronal sections of GFP (green), tdTomato (red), and SST or PV (blue). Arrows point to cells expressing either SST or PV, and both GFP and tdTomato; asterisks mark cells only expressing tdTomato. Scale bar represents 100 μm.

(E) Model of *Lhx6* actions. *Lhx6* represses CGE-like interneuron fate. Lhx6 directly binds to enhancers near *Arx* and *CXCR7* to promote expression of these genes. ARX and CXCR7 are sufficient to rescue *Lhx6*$^{PLAP/PLAP}$ MGE cell fate (SST and PV expression) and laminar distribution, respectively. Data are expressed as mean ± SEM. One-way ANOVA was used to test significance between groups. *$p < 0.05$, **$p < 0.01$.

See also Figure S8.

and this enhancer remained active in mature GABAergic interneurons, allowing for assessment at multiple stages of development.

Either *Lhx6* or *Lhx8* transduction can rescue the *Lhx6*$^{PLAP/PLAP}$ phenotypes (Figure 4). Despite transducing cells at E13.5, ~3 days after the MGE would normally begin to express *Lhx6*, the mutant MGE cells maintained sufficient plasticity to be rescued. *Lhx8* transduction in *Lhx6*$^{PLAP/PLAP}$ cortical interneurons enabled them to express PV and SST; thus *Lhx6* and *Lhx8* share some common functions. Interestingly, forced expression of Lhx8 in cortical interneurons restored features associated with Lhx6 expression (Sox6, PV, and SST) rather than inducing cholinergic markers (ChAT) (Figure S4), suggesting that other cofactors may distinguish the cholinergic and GABAergic lineages (e.g., *Isl1* is implicated in the telencephalic cholinergic differentiation) (Elshatory and Gan, 2008; Fragkouli et al., 2009).

Arx transduction into *Lhx6* mutants was sufficient to rescue both SST and PV expression, but it was more efficient at promoting PV$^+$ interneurons (Figure 4). This difference could be due to the inability of *Arx* to rescue *Satb1* expression in *Lhx6* mutants (Figure S5), as *Satb1* function in MGE interneurons is linked to SST expression (Denaxa et al., 2012; Close et al., 2012).

Arx could promote interneuron differentiation through several molecular pathways. The *Drosophila* Arx (Aristaless) protein binds to Chip, an invertebrate homolog of mammalian Ldb1 (Pueyo and Couso, 2004). Ldb1 is an essential cofactor for Lim-domain homeodomain proteins such as Islet-1, Lhx8, and Lhx6 (Kimura et al., 1999; Y. Zhao and J.L.R.R., unpublished data). Second, in developing muscle, ARX can form a complex with, and enhance the activity of the Mef2C TF (Biressi et al., 2008). Mef2C may have roles in cortical interneuron maturation, as its expression in GABAergic neurons is reduced in *Dlx1/2*$^{-/-}$ mutants (Cobos et al., 2007; Long et al., 2009). Thus, Arx may modulate interneuron cell fate through association with Ldb1, Mef2C, or other factors.

Surprisingly, *Sox6* was not sufficient to rescue the *Lhx6* null phenotypes (Figure 4), although *Sox6* is required for development of MGE-derived cortical interneurons (Azim et al., 2009; Batista-Brito et al., 2009). One possibility is that the actions of Sox6 require Lhx6 expression. On the other hand, expression of *Sox6* in control MGE cells increased the ratio of SST/PV-expressing interneurons (Figure 4 and data not shown), suggesting that Sox6 dosage regulates the balance of interneuron subgroups. These data may be of use in furthering methods to program stem cells into specific subgroups of MGE-derived cortical interneurons (Chen et al., 2013; Maroof et al., 2013; Nicholas et al., 2013).

CXCR7 Is a Direct Target of Lhx6 and Modulates Laminar Positioning of Transplanted Interneurons

While *Arx* rescued MGE cell fate, it could not rescue the *Lhx6* mutant lamination phenotype (Liodis et al., 2007; Zhao et al., 2008), in which ~45% of the transplanted mutant interneurons populate neocortical layer I (Figure 5). We propose two mechanisms to explain this abnormal lamination pattern. First, some of these cells exhibit a fate change, acquiring properties of a subset of CGE-derived interneurons that occupy neocortical layer I (Miyoshi et al., 2010). It is also possible that they become POA-like neurogliaform cells (Gelman et al., 2011), although this is less likely based on their expression of Sp8 (Figure 1).

The second mechanism potentially underlying the lamination phenotype is the reduced expression of the CXCR7 and CXCR4 chemokine receptors in *Lhx6* mutant interneurons migrating in the cortex (Zhao et al., 2008). CXCR7 regulates interneuron tangential and radial migration and is required to prevent degradation of CXCR4 (Sánchez-Alcañiz et al., 2011; Wang et al., 2011). We found that transduction of *CXCR7* in *Lhx6* mutants partially rescued the ability of interneurons to exit layer I and integrate into deeper neocortical layers, independent of changes in cell fate (Figures 4 and 5). Transplanted *CXCR4*$^{-/-}$ and *CXCR7*$^{-/-}$ MGE cells were less represented in layer V (Figure 6), suggesting that these receptors participate in radial migration and laminar targeting in the postnatal neocortex. We and others have observed postnatal expression of CXCL12, a CXCR4/7 ligand and interneuron attractant, in layer V pyramidal neurons (Schönemeier et al., 2008; Tiveron et al., 2006; Wang et al., 2011). We hypothesize that postnatal CXCL12 may influence the laminar position of cortical interneurons. However, we are cognizant that the transplantation assay we employed does not recapitulate the normal developmental sequence followed by interneurons; thus in vivo genetic manipulations are needed to test this model. For example, one would selectively eliminate *CXCL12* function in developing layer V, and not in the other locations where it is expressed (marginal and intermediate zones) and then examine interneuron laminar positioning. Ideally, this would be done by deleting CXCL12 at a specific time and cell type (i.e., only in early postnatal layer V pyramidal neurons).

Use of the MGE Complementation Assay to Determine Gene Functions, Coding and Regulatory, in Interneuron Development

We propose that the MGE complementation assay has broad utility to elucidate in vivo functions of candidate alleles. MGE cells are ideally suited for this approach because they can be harvested prenatally, easily transduced, and transplanted in the cortex, where they migrate, differentiate, and functionally integrate (Alvarez-Dolado et al., 2006). This type of complementation and MGE transplantation assay was used to assess the role of Lhx6 in the *Nkx2.1* mutant (Du et al., 2008). Here, we modified this approach by transducing genes using lentiviruses with enhancer elements that drive expression specifically in GABAergic neurons. Importantly, this assay can be used to test the functions of WT genes whose expression is downregulated in a given mutant (as in this article and Du et al., 2008). Alternatively, one can compare the ability of mutant alleles, discovered in human genetic analyses of neuropsychiatric disorders, to rescue phenotypes as compared to WT alleles. Thus, this technique provides a powerful in vivo approach to test a number of molecular mechanisms.

Furthermore, this approach can be used to assay enhancers. Previously, we presented evidence that Lhx6, with Lhx8, regulates a forebrain *Shh* enhancer in MGE neurons (Flandin et al., 2011). Here, we have shown that Lhx6 directly regulates two genes whose functions substantively contribute to the

Lhx6 null phenotype: *Arx* and *CXCR7*. Chromatin immunoprecipitation-quantitative PCR (ChIP-qPCR) data identified Lhx6 binding to a previously known *Arx* subpallial enhancer (also regulated by Dlx2) (Colasante et al., 2008), and a *CXCR7* enhancer (Figure 7). This enhancer preferentially drives expression in the MGE, compared to the other basal ganglia primordia (Figure S8). Moreover, by using the MGE-transplantation assay to assess cells transduced with the *CXCR7* enhancer, we found that it drives expression in SST and PV interneurons into adulthood (Figure 7). We propose that this approach to assay enhancer functions will accelerate the identification of regulatory elements that control expression in immature and mature cortical interneurons and should be useful to test the activity of enhancer variants discovered in human genetic analyses of neuropsychiatric disorders.

EXPERIMENTAL PROCEDURES

Animals

Mice were maintained on a CD-1 background. For timed pregnancies, noon on the day of the vaginal plug was counted as embryonic day 0.5. All mice strains have been previously reported: *AI14* Cre-reporter (Madisen et al., 2010), *CXCL-12-GFP* (Ara et al., 2003), *CXCR7*$^{-/-}$ (Sierro et al., 2007), *CXCR4*$^{-/-}$ (Jackson Laboratory 004341), *Lhx6-PLAP* (Choi et al., 2005), *Lhx6 BAC-GFP* (GENSAT), and *Nkx2-1-Cre* (Xu et al., 2008). All animal care and procedures were performed according to the University of California at San Francisco Laboratory Animal Research Center guidelines.

ChIP-qPCR

ChIP was performed on E13.5 basal ganglia using ~4 μg of Lhx6 polyclonal antibody (Genscript), and 20-fold excess of blocking peptide used as a negative control. The antibody/protein complexes were processed according to the Millipore-Upstate ChIP protocol, and qPCR analyzed as described (Vokes et al., 2007). See the Supplemental Experimental Procedures for detailed methods.

Electrophysiology

Coronal sections were prepared from P35 transplanted mice and assessed as described in Hunt et al. (2013). See the Supplemental Experimental Procedures for detailed methods.

Histology

In situ hybridization on 20 um cryosections was performed as previously described (Jeong et al., 2008). Immunofluorescence was performed on 25 um cryosection as previously described (Zhao et al., 2008). See the Supplemental Experimental Procedures for list of probes, detailed methods, and reagents.

Image Acquisition and Analysis

Fluorescent images were taken using a Coolsnap camera (Photometrics) mounted on a Nikon Eclipse 80i microscope using NIS Elements acquisition software (Nikon). Brightfield images were taken using a DP70 camera (Olympus) mounted to an Olympus SZX7 microscope. Brightness and contrast were adjusted and images merged using ImageJ software.

In Situ Hybridization

Coronal cryostat sections were prepared and processed as described in Jeong et al. (2008). Briefly, E15.5 brains were fixed in 4% paraformaldehyde (PFA) then sunk in 30% sucrose before cutting 20 μm sections. The Sp8 probe has been previously reported (C. Belmonte).

Lentiviral Production

HEK293T cells grown in DMEM H21 with 10% FBS were transfected using Fugene 6 (Promega) with the lentiviral vector and three helper plasmids (pVSV-g, pRSVr, and pMDLg-pRRE). Media was filtered after 4 days in culture and ultracentrifuged at 100,000 × *g* for 2.5 hr at 4°C and the lentiviral pellet resuspended in PBS before use. See the Supplemental Experimental Procedures for details on lentiviral vectors.

Luciferase Assays

P19 cells were seeded at density of 100,000 cells/cm^2 in MEM + nucleosides supplemented with 2.5% FBS and 7.5% CS. Cells were transfected at 24 hr with 500 ng total of a DNA mix containing firefly luciferase, transcription factor, and Renilla luciferase vectors. Cells were harvested 48 hr later and assessed for luciferase activity according to Dual luciferase-reproter assay system protocol (Promega).

MGE Transplantation

E13.5 MGE transplantations were done as previously described (Alvarez-Dolado et al., 2006; Cobos et al., 2005). Briefly, MGEs were mechanically dissociated, pelleted, and transplanted into P1 host neocortices or transduced with concentrated lentivirus before transplantation. For transduction, MGE cells were incubated with lentivirus in media for 30 min at 37°C and then washed with media three times before transplantation. Each host received three to four injections of ~70 nl per site. See the Supplemental Experimental Procedures for detailed methods.

SUPPLEMENTAL INFORMATION

Supplemental Information includes Supplemental Experimental Procedures, eight figures, and one table and can be found with this article online at http://dx.doi.org/10.1016/j.neuron.2014.02.030.

ACKNOWLEDGMENTS

This work was supported by grants to J.L.R.R. from Autism Speaks, Nina Ireland, Weston Havens Foundation, and the National Institute of Mental Health (NIMH) (R01 MH081880 and R37 MH049428). The National Institute of Neurological Disorders and Stroke (NINDS) provided grants to S.C.B. (R01NS071785) and R.F.H. (F32NS077747). We thank Grant Li, Pierre Flandin, Jasmine Chen, Ramon Pla, and Katherine Krueger for advice and critical evaluation of the data.

Accepted: February 11, 2014
Published: April 16, 2014

REFERENCES

Alcántara, S., Ruiz, M., D'Arcangelo, G., Ezan, F., de Lecea, L., Curran, T., Sotelo, C., and Soriano, E. (1998). Regional and cellular patterns of reelin mRNA expression in the forebrain of the developing and adult mouse. J. Neurosci. *18*, 7779–7799.

Alvarez-Dolado, M., Calcagnotto, M.E., Karkar, K.M., Southwell, D.G., Jones-Davis, D.M., Estrada, R.C., Rubenstein, J.L.R., Alvarez-Buylla, A., and Baraban, S.C. (2006). Cortical inhibition modified by embryonic neural precursors grafted into the postnatal brain. J. Neurosci. *26*, 7380–7389.

Anderson, S.A., Eisenstat, D.D., Shi, L., and Rubenstein, J.L.R. (1997). Interneuron migration from basal forebrain to neocortex: dependence on Dlx genes. Science *278*, 474–476.

Ara, T., Tokoyoda, K., Sugiyama, T., Egawa, T., Kawabata, K., and Nagasawa, T. (2003). Long-term hematopoietic stem cells require stromal cell-derived factor-1 for colonizing bone marrow during ontogeny. Immunity *19*, 257–267.

Arguello, A., Yang, X., Vogt, D., Stanco, A., Rubenstein, J.L., and Cheyette, B.N. (2013). Dapper antagonist of catenin-1 cooperates with Dishevelled-1 during postsynaptic development in mouse forebrain GABAergic interneurons. PLoS ONE *8*, e67679.

Armstrong, C., Szabadics, J., Tamás, G., and Soltesz, I. (2011). Neurogliaform cells in the molecular layer of the dentate gyrus as feed-forward γ-aminobutyric

acidergic modulators of entorhinal-hippocampal interplay. J. Comp. Neurol. *519*, 1476–1491.

Azim, E., Jabaudon, D., Fame, R.M., and Macklis, J.D. (2009). SOX6 controls dorsal progenitor identity and interneuron diversity during neocortical development. Nat. Neurosci. *12*, 1238–1247.

Batista-Brito, R., Rossignol, E., Hjerling-Leffler, J., Denaxa, M., Wegner, M., Lefebvre, V., Pachnis, V., and Fishell, G. (2009). The cell-intrinsic requirement of Sox6 for cortical interneuron development. Neuron *63*, 466–481.

Biressi, S., Messina, G., Collombat, P., Tagliafico, E., Monteverde, S., Benedetti, L., Cusella De Angelis, M.G., Mansouri, A., Ferrari, S., Tajbakhsh, S., et al. (2008). The homeobox gene Arx is a novel positive regulator of embryonic myogenesis. Cell Death Differ. *15*, 94–104.

Cai, Y., Zhang, Q., Wang, C., Zhang, Y., Ma, T., Zhou, X., Tian, M., Rubenstein, J.L., and Yang, Z. (2013). Nuclear receptor COUP-TFII-expressing neocortical interneurons are derived from the medial and lateral/caudal ganglionic eminence and define specific subsets of mature interneurons. J. Comp. Neurol. *521*, 479–497.

Chao, H.T., Chen, H., Samaco, R.C., Xue, M., Chahrour, M., Yoo, J., Neul, J.L., Gong, S., Lu, H.C., Heintz, N., et al. (2010). Dysfunction in GABA signalling mediates autism-like stereotypies and Rett syndrome phenotypes. Nature *468*, 263–269.

Chen, Y.J., Vogt, D., Wang, Y., Visel, A., Silberberg, S.N., Nicholas, C.R., Danjo, T., Pollack, J.L., Pennacchio, L.A., Anderson, S., et al. (2013). Use of "MGE enhancers" for labeling and selection of embryonic stem cell-derived medial ganglionic eminence (MGE) progenitors and neurons. PLoS ONE *8*, e61956.

Choi, G.B., Dong, H.-W., Murphy, A.J., Valenzuela, D.M., Yancopoulos, G.D., Swanson, L.W., and Anderson, D.J. (2005). Lhx6 delineates a pathway mediating innate reproductive behaviors from the amygdala to the hypothalamus. Neuron *46*, 647–660.

Chu, Z., Galarreta, M., and Hestrin, S. (2003). Synaptic interactions of late-spiking neocortical neurons in layer 1. J. Neurosci. *23*, 96–102.

Close, J., Xu, H., De Marco García, N., Batista-Brito, R., Rossignol, E., Rudy, B., and Fishell, G. (2012). Satb1 is an activity-modulated transcription factor required for the terminal differentiation and connectivity of medial ganglionic eminence-derived cortical interneurons. J. Neurosci. *32*, 17690–17705.

Cobos, I., Calcagnotto, M.E., Vilaythong, A.J., Thwin, M.T., Noebels, J.L., Baraban, S.C., and Rubenstein, J.L.R. (2005). Mice lacking Dlx1 show subtype-specific loss of interneurons, reduced inhibition and epilepsy. Nat. Neurosci. *8*, 1059–1068.

Cobos, I., Borello, U., and Rubenstein, J.L.R. (2007). Dlx transcription factors promote migration through repression of axon and dendrite growth. Neuron *54*, 873–888.

Colasante, G., Collombat, P., Raimondi, V., Bonanomi, D., Ferrai, C., Maira, M., Yoshikawa, K., Mansouri, A., Valtorta, F., Rubenstein, J.L.R., and Broccoli, V. (2008). Arx is a direct target of Dlx2 and thereby contributes to the tangential migration of GABAergic interneurons. J. Neurosci. *28*, 10674–10686.

Denaxa, M., Kalaitzidou, M., Garefalaki, A., Achimastou, A., Lasrado, R., Maes, T., and Pachnis, V. (2012). Maturation-promoting activity of SATB1 in MGE-derived cortical interneurons. Cell Rep. *2*, 1351–1362.

Du, T., Xu, Q., Ocbina, P.J., and Anderson, S.A. (2008). NKX2.1 specifies cortical interneuron fate by activating Lhx6. Development *135*, 1559–1567.

Elshatory, Y., and Gan, L. (2008). The LIM-homeobox gene Islet-1 is required for the development of restricted forebrain cholinergic neurons. J. Neurosci. *28*, 3291–3297.

Flandin, P., Kimura, S., and Rubenstein, J.L. (2010). The progenitor zone of the ventral medial ganglionic eminence requires Nkx2-1 to generate most of the globus pallidus but few neocortical interneurons. J. Neurosci. *30*, 2812–2823.

Flandin, P., Zhao, Y., Vogt, D., Jeong, J., Long, J., Potter, G., Westphal, H., and Rubenstein, J.L.R. (2011). Lhx6 and Lhx8 coordinately induce neuronal expression of Shh that controls the generation of interneuron progenitors. Neuron *70*, 939–950.

Fragkouli, A., van Wijk, N.V., Lopes, R., Kessaris, N., and Pachnis, V. (2009). LIM homeodomain transcription factor-dependent specification of bipotential MGE progenitors into cholinergic and GABAergic striatal interneurons. Development *136*, 3841–3851.

Gelman, D., Griveau, A., Dehorter, N., Teissier, A., Varela, C., Pla, R., Pierani, A., and Marín, O. (2011). A wide diversity of cortical GABAergic interneurons derives from the embryonic preoptic area. J. Neurosci. *31*, 16570–16580.

Ghanem, N., Jarinova, O., Amores, A., Long, Q., Hatch, G., Park, B.K., Rubenstein, J.L., and Ekker, M. (2003). Regulatory roles of conserved intergenic domains in vertebrate Dlx bigene clusters. Genome Res. *13*, 533–543.

Grigoriou, M., Tucker, A.S., Sharpe, P.T., and Pachnis, V. (1998). Expression and regulation of Lhx6 and Lhx7, a novel subfamily of LIM homeodomain encoding genes, suggests a role in mammalian head development. Development *125*, 2063–2074.

Han, S., Tai, C., Westenbroek, R.E., Yu, F.H., Cheah, C.S., Potter, G.B., Rubenstein, J.L., Scheuer, T., de la Iglesia, H.O., and Catterall, W.A. (2012). Autistic-like behaviour in Scn1a+/- mice and rescue by enhanced GABA-mediated neurotransmission. Nature *489*, 385–390.

Huang, Z.J., Di Cristo, G., and Ango, F. (2007). Development of GABA innervation in the cerebral and cerebellar cortices. Nat. Rev. Neurosci. *8*, 673–686.

Hunt, R.F., Girskis, K.M., Rubenstein, J.L., Alvarez-Buylla, A., and Baraban, S.C. (2013). GABA progenitors grafted into the adult epileptic brain control seizures and abnormal behavior. Nat. Neurosci. *16*, 692–697.

Jeong, J., Li, X., McEvilly, R.J., Rosenfeld, M.G., Lufkin, T., and Rubenstein, J.L. (2008). Dlx genes pattern mammalian jaw primordium by regulating both lower jaw-specific and upper jaw-specific genetic programs. Development *135*, 2905–2916.

Kanatani, S., Yozu, M., Tabata, H., and Nakajima, K. (2008). COUP-TFII is preferentially expressed in the caudal ganglionic eminence and is involved in the caudal migratory stream. J. Neurosci. *28*, 13582–13591.

Kimura, N., Ueno, M., Nakashima, K., and Taga, T. (1999). A brain region-specific gene product Lhx6.1 interacts with Ldb1 through tandem LIM-domains. J. Biochem. *126*, 180–187.

Lee, S., Hjerling-Leffler, J., Zagha, E., Fishell, G., and Rudy, B. (2010). The largest group of superficial neocortical GABAergic interneurons expresses ionotropic serotonin receptors. J. Neurosci. *30*, 16796–16808.

Liodis, P., Denaxa, M., Grigoriou, M., Akufo-Addo, C., Yanagawa, Y., and Pachnis, V. (2007). Lhx6 activity is required for the normal migration and specification of cortical interneuron subtypes. J. Neurosci. *27*, 3078–3089.

Long, J.E., Cobos, I., Potter, G.B., and Rubenstein, J.L.R. (2009). Dlx1&2 and Mash1 transcription factors control MGE and CGE patterning and differentiation through parallel and overlapping pathways. Cereb. Cortex *19* (*Suppl 1*), i96–i106.

Ma, T., Zhang, Q., Cai, Y., You, Y., Rubenstein, J.L.R., and Yang, Z. (2012). A subpopulation of dorsal lateral/caudal ganglionic eminence-derived neocortical interneurons expresses the transcription factor Sp8. Cereb. Cortex *22*, 2120–2130.

Madisen, L., Zwingman, T.A., Sunkin, S.M., Oh, S.W., Zariwala, H.A., Gu, H., Ng, L.L., Palmiter, R.D., Hawrylycz, M.J., Jones, A.R., et al. (2010). A robust and high-throughput Cre reporting and characterization system for the whole mouse brain. Nat. Neurosci. *13*, 133–140.

Maroof, A.M., Keros, S., Tyson, J.A., Ying, S.W., Ganat, Y.M., Merkle, F.T., Liu, B., Goulburn, A., Stanley, E.G., Elefanty, A.G., et al. (2013). Directed differentiation and functional maturation of cortical interneurons from human embryonic stem cells. Cell Stem Cell *12*, 559–572.

McKinsey, G.L., Lindtner, S., Trzcinski, B., Visel, A., Pennacchio, L.A., Huylebroeck, D., Higashi, Y., and Rubenstein, J.L. (2013). Dlx1&2-dependent expression of Zfhx1b (Sip1, Zeb2) regulates the fate switch between cortical and striatal interneurons. Neuron *77*, 83–98.

Miyoshi, G., and Fishell, G. (2011). GABAergic interneuron lineages selectively sort into specific cortical layers during early postnatal development. Cereb. Cortex *21*, 845–852.

Miyoshi, G., Hjerling-Leffler, J., Karayannis, T., Sousa, V.H., Butt, S.J.B., Battiste, J., Johnson, J.E., Machold, R.P., and Fishell, G. (2010). Genetic fate mapping reveals that the caudal ganglionic eminence produces a large and diverse population of superficial cortical interneurons. J. Neurosci. *30*, 1582–1594.

Nicholas, C.R., Chen, J., Tang, Y., Southwell, D.G., Chalmers, N., Vogt, D., Arnold, C.M., Chen, Y.J., Stanley, E.G., Elefanty, A.G., et al. (2013). Functional maturation of hPSC-derived forebrain interneurons requires an extended timeline and mimics human neural development. Cell Stem Cell *12*, 573–586.

Potter, G.B., Petryniak, M.A., Shevchenko, E., McKinsey, G.L., Ekker, M., and Rubenstein, J.L.R. (2009). Generation of Cre-transgenic mice using Dlx1/Dlx2 enhancers and their characterization in GABAergic interneurons. Mol. Cell. Neurosci. *40*, 167–186.

Pueyo, J.I., and Couso, J.P. (2004). Chip-mediated partnerships of the homeodomain proteins Bar and Aristaless with the LIM-HOM proteins Apterous and Lim1 regulate distal leg development. Development *131*, 3107–3120.

Rubenstein, J.L., and Merzenich, M.M. (2003). Model of autism: increased ratio of excitation/inhibition in key neural systems. Genes Brain Behav. *2*, 255–267.

Rudy, B., Fishell, G., Lee, S., and Hjerling-Leffler, J. (2011). Three groups of interneurons account for nearly 100% of neocortical GABAergic neurons. Dev. Neurobiol. *71*, 45–61.

Sánchez-Alcañiz, J.A., Haege, S., Mueller, W., Pla, R., Mackay, F., Schulz, S., López-Bendito, G., Stumm, R., and Marín, O. (2011). Cxcr7 controls neuronal migration by regulating chemokine responsiveness. Neuron *69*, 77–90.

Schönemeier, B., Kolodziej, A., Schulz, S., Jacobs, S., Hoellt, V., and Stumm, R. (2008). Regional and cellular localization of the CXCl12/SDF-1 chemokine receptor CXCR7 in the developing and adult rat brain. J. Comp. Neurol. *510*, 207–220.

Sierro, F., Biben, C., Martínez-Muñoz, L., Mellado, M., Ransohoff, R.M., Li, M., Woehl, B., Leung, H., Groom, J., Batten, M., et al. (2007). Disrupted cardiac development but normal hematopoiesis in mice deficient in the second CXCL12/SDF-1 receptor, CXCR7. Proc. Natl. Acad. Sci. USA *104*, 14759–14764.

Stumm, R.K., Zhou, C., Ara, T., Lazarini, F., Dubois-Dalcq, M., Nagasawa, T., Höllt, V., and Schulz, S. (2003). CXCR4 regulates interneuron migration in the developing neocortex. J. Neurosci. *23*, 5123–5130.

Sussel, L., Marin, O., Kimura, S., and Rubenstein, J.L. (1999). Loss of Nkx2.1 homeobox gene function results in a ventral to dorsal molecular respecification within the basal telencephalon: evidence for a transformation of the pallidum into the striatum. Development *126*, 3359–3370.

Tiveron, M.C., Rossel, M., Moepps, B., Zhang, Y.L., Seidenfaden, R., Favor, J., König, N., and Cremer, H. (2006). Molecular interaction between projection neuron precursors and invading interneurons via stromal-derived factor 1 (CXCL12)/CXCR4 signaling in the cortical subventricular zone/intermediate zone. J. Neurosci. *26*, 13273–13278.

Tricoire, L., Pelkey, K.A., Daw, M.I., Sousa, V.H., Miyoshi, G., Jeffries, B., Cauli, B., Fishell, G., and McBain, C.J. (2010). Common origins of hippocampal Ivy and nitric oxide synthase expressing neurogliaform cells. J. Neurosci. *30*, 2165–2176.

Tricoire, L., Pelkey, K.A., Erkkila, B.E., Jeffries, B.W., Yuan, X., and McBain, C.J. (2011). A blueprint for the spatiotemporal origins of mouse hippocampal interneuron diversity. J. Neurosci. *31*, 10948–10970.

Vintersten, K., Monetti, C., Gertsenstein, M., Zhang, P., Laszlo, L., Biechele, S., and Nagy, A. (2004). Mouse in red: red fluorescent protein expression in mouse ES cells, embryos, and adult animals. Genesis *40*, 241–246.

Vokes, S.A., Ji, H., McCuine, S., Tenzen, T., Giles, S., Zhong, S., Longabaugh, W.J.R., Davidson, E.H., Wong, W.H., and McMahon, A.P. (2007). Genomic characterization of Gli-activator targets in sonic hedgehog-mediated neural patterning. Development *134*, 1977–1989.

Wang, Y., Li, G., Stanco, A., Long, J.E., Crawford, D., Potter, G.B., Pleasure, S.J., Behrens, T., and Rubenstein, J.L.R. (2011). CXCR4 and CXCR7 have distinct functions in regulating interneuron migration. Neuron *69*, 61–76.

Wonders, C.P., and Anderson, S.A. (2006). The origin and specification of cortical interneurons. Nat. Rev. Neurosci. *7*, 687–696.

Xu, Q., Tam, M., and Anderson, S.A. (2008). Fate mapping Nkx2.1-lineage cells in the mouse telencephalon. J. Comp. Neurol. *506*, 16–29.

Yizhar, O., Fenno, L.E., Prigge, M., Schneider, F., Davidson, T.J., O'Shea, D.J., Sohal, V.S., Goshen, I., Finkelstein, J., Paz, J.T., et al. (2011). Neocortical excitation/inhibition balance in information processing and social dysfunction. Nature *477*, 171–178.

Zerucha, T., Stuhmer, T., Hatch, G., Park, B.K., Long, Q., Yu, G., Gambarotta, A., Schultz, J.R., Rubenstein, J.L., and Ekker, M. (2000). A highly conserved enhancer in the Dlx5/Dlx6 intergenic region is the site of cross-regulatory interactions between Dlx genes in the embryonic forebrain. J. Neurosci. *20*, 709–721.

Zhao, Y., Marín, O., Hermesz, E., Powell, A., Flames, N., Palkovits, M., Rubenstein, J.L., and Westphal, H. (2003). The LIM-homeobox gene Lhx8 is required for the development of many cholinergic neurons in the mouse forebrain. Proc. Natl. Acad. Sci. USA *100*, 9005–9010.

Zhao, Y., Flandin, P., Long, J.E., Cuesta, M.D., Westphal, H., and Rubenstein, J.L.R. (2008). Distinct molecular pathways for development of telencephalic interneuron subtypes revealed through analysis of Lhx6 mutants. J. Comp. Neurol. *510*, 79–99.

Zhou, F.M., and Hablitz, J.J. (1997). Rapid kinetics and inward rectification of miniature EPSCs in layer I neurons of rat neocortex. J. Neurophysiol. *77*, 2416–2426.

Neuron, Volume *82*

Supplemental Information

Lhx6 Directly Regulates *Arx* and *CXCR7* to Determine Cortical Interneuron Fate and Laminar Position

Daniel Vogt, Robert F. Hunt, Shyamali Mandal, Magnus Sandberg, Shanni N. Silberberg, Takashi Nagasawa, Zhengang Yang, Scott C. Baraban, and John L.R. Rubenstein

Supplemental Figures:

Figure S1

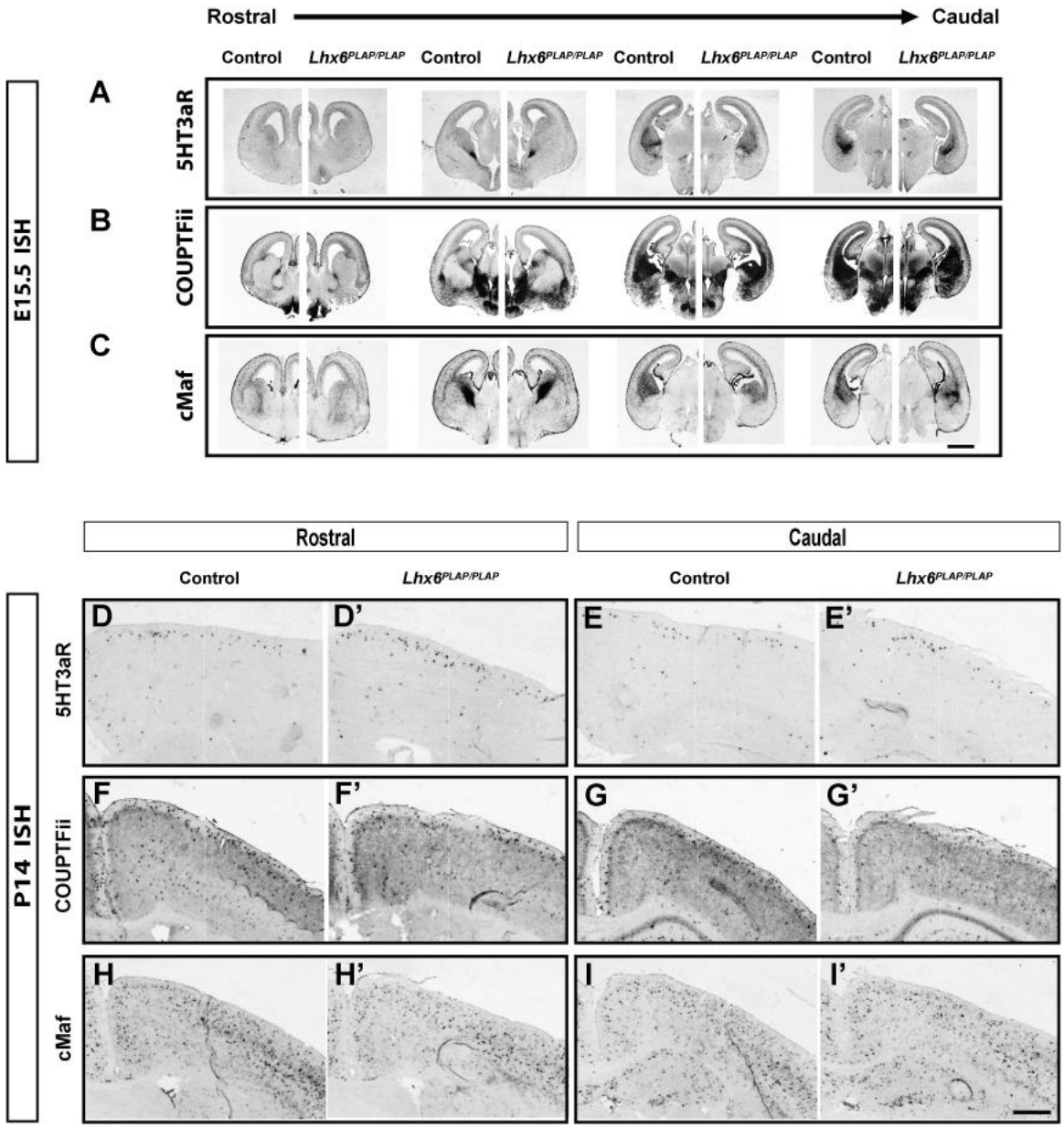

Figure S2

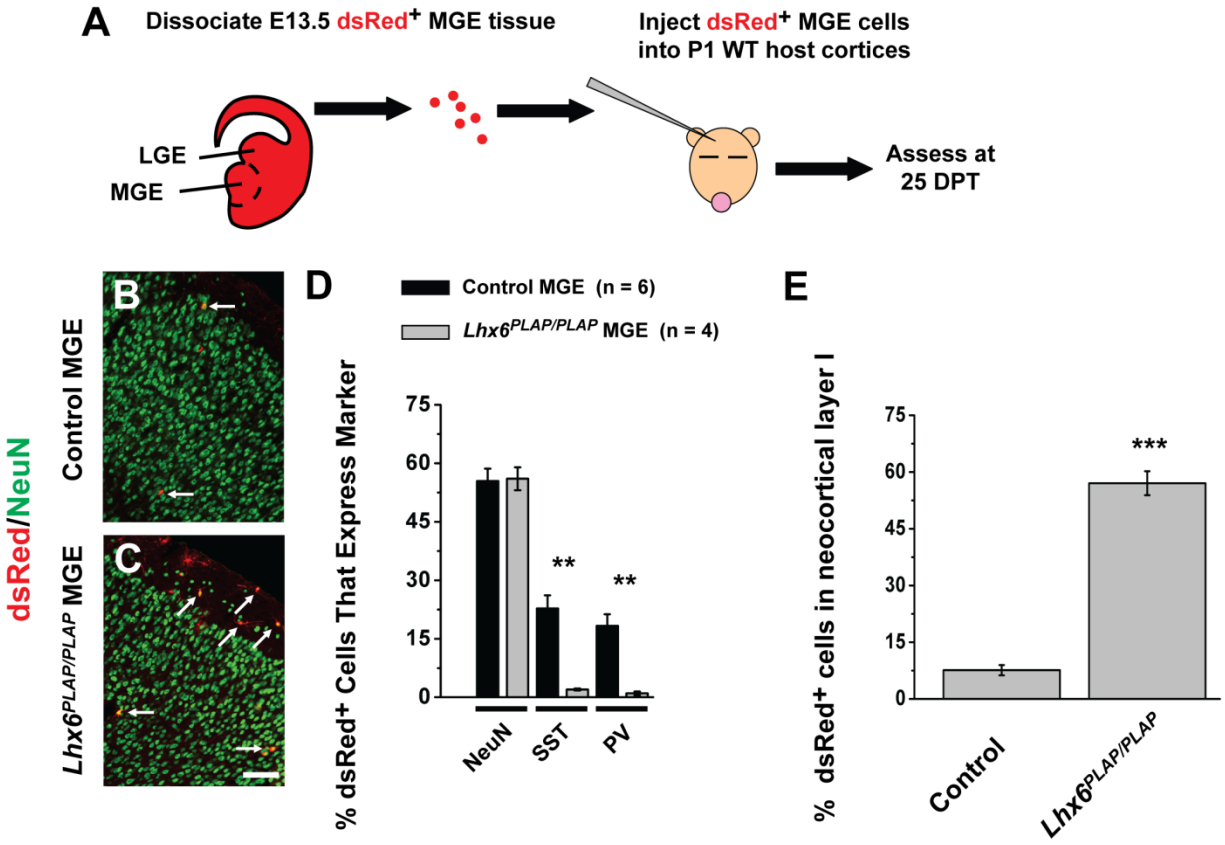
A
Dissociate E13.5 dsRed+ MGE tissue
Inject dsRed+ MGE cells into P1 WT host cortices
LGE
MGE
Assess at 25 DPT
dsRed/NeuN
Control MGE
Lhx6PLAP/PLAP MGE
B
C
D
Control MGE (n = 6)
Lhx6PLAP/PLAP MGE (n = 4)
% dsRed+ Cells That Express Marker
75
60
45
30
15
0
**
**
NeuN
SST
PV
E
% dsRed+ cells in neocortical layer I
***
Control
Lhx6PLAP/PLAP

Figure S3

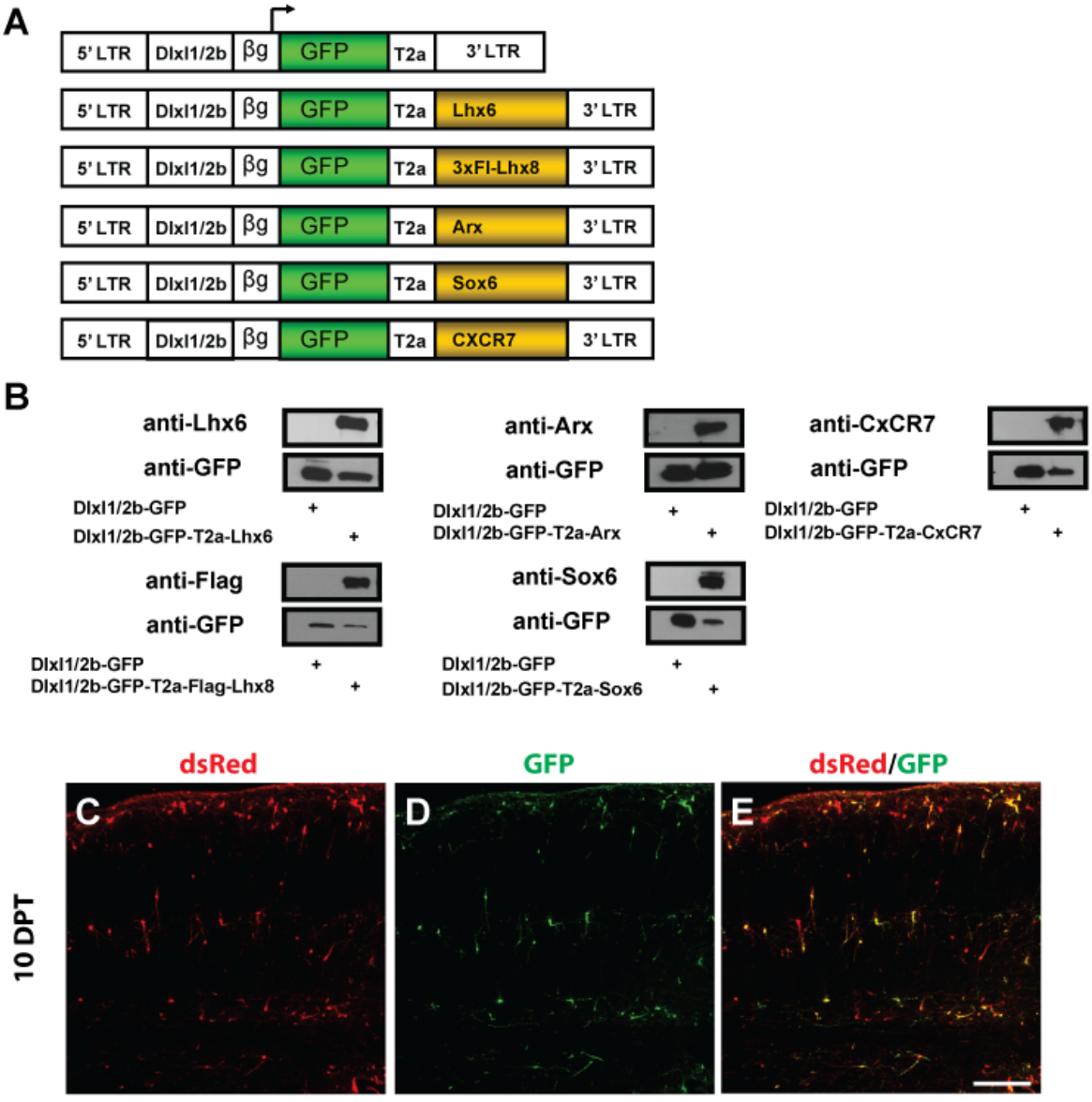
A
5' LTR
Dlxl1/2b
βg
GFP
T2a
3' LTR
Lhx6
3xFl-Lhx8
Arx
Sox6
CXCR7
B
anti-Lhx6
anti-GFP
Dlxl1/2b-GFP
Dlxl1/2b-GFP-T2a-Lhx6
anti-Arx
Dlxl1/2b-GFP-T2a-Arx
anti-CxCR7
Dlxl1/2b-GFP-T2a-CxCR7
anti-Flag
Dlxl1/2b-GFP-T2a-Flag-Lhx8
anti-Sox6
Dlxl1/2b-GFP-T2a-Sox6
dsRed
GFP
dsRed/GFP
C
D
E
10 DPT

Figure S4

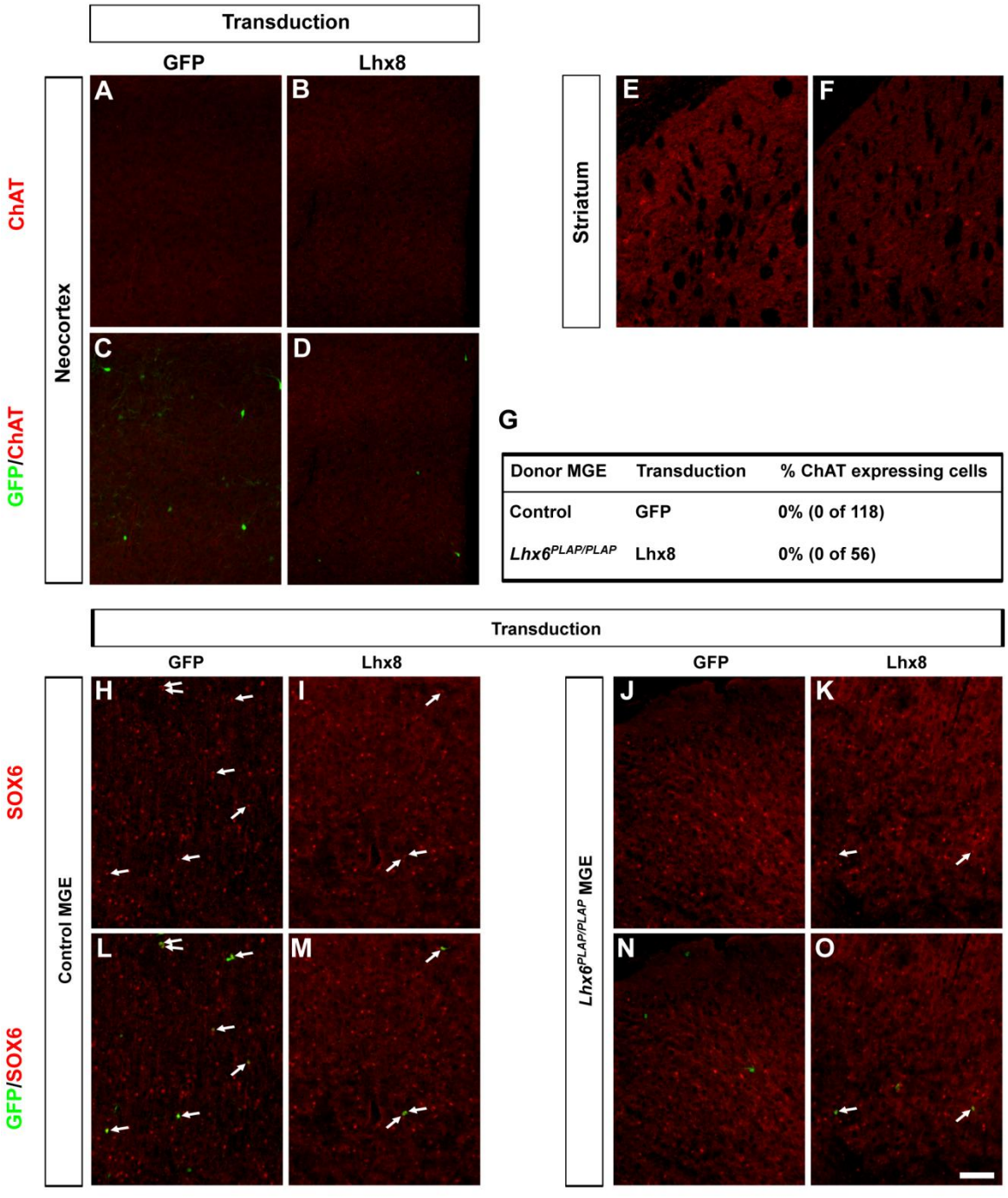

G

Donor MGE	Transduction	% ChAT expressing cells
Control	GFP	0% (0 of 118)
Lhx6$^{PLAP/PLAP}$	Lhx8	0% (0 of 56)

P

Donor MGE	Transduction	% SOX6 expressing cells
Control	GFP	73.9% (85 of 115)
Control	Lhx8	87.2% (41 of 47)

Q

Donor MGE	Transduction	% SOX6 expressing cells
Lhx6$^{PLAP/PLAP}$	GFP	5.3% (4 of 75)
Lhx6$^{PLAP/PLAP}$	Lhx8	58.8% (47 of 80)

Figure S5

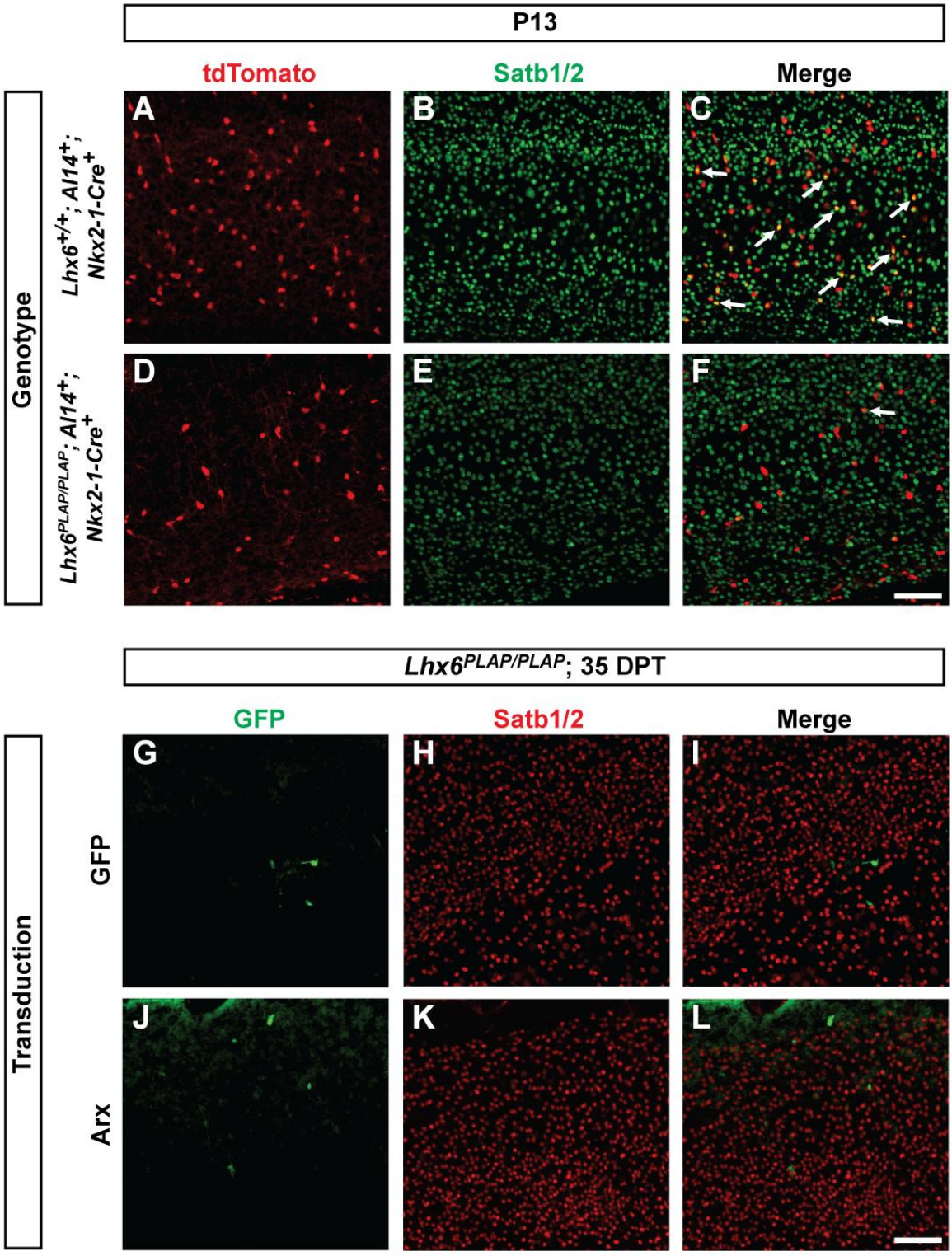
P13
tdTomato
Satb1/2
Merge
Genotype
Lhx6+/+; Al14+; Nkx2-1-Cre+
Lhx6PLAP/PLAP; Al14+; Nkx2-1-Cre+
A
B
C
D
E
F
Lhx6PLAP/PLAP; 35 DPT
GFP
Satb1/2
Merge
Transduction
GFP
Arx
G
H
I
J
K
L

Figure S6

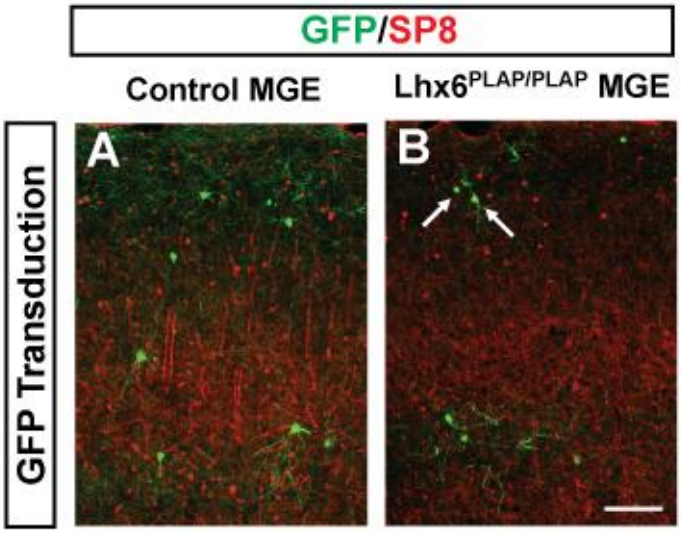

Figure S7

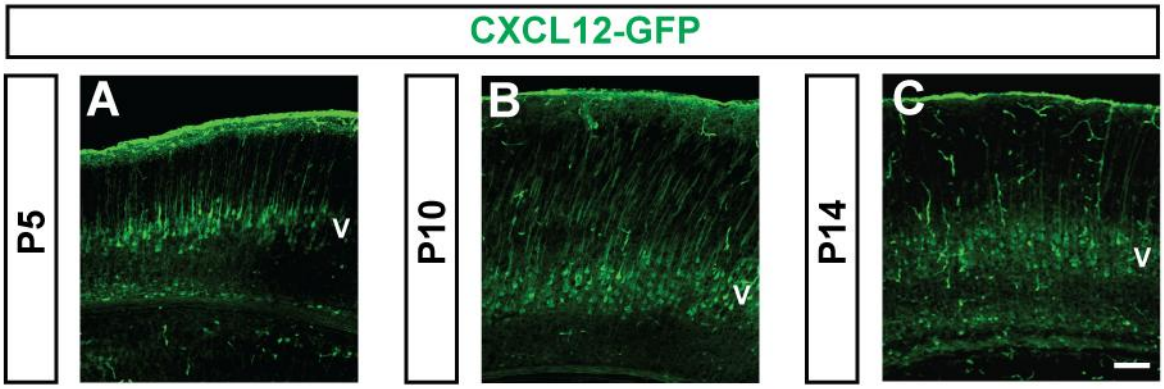

Figure S8

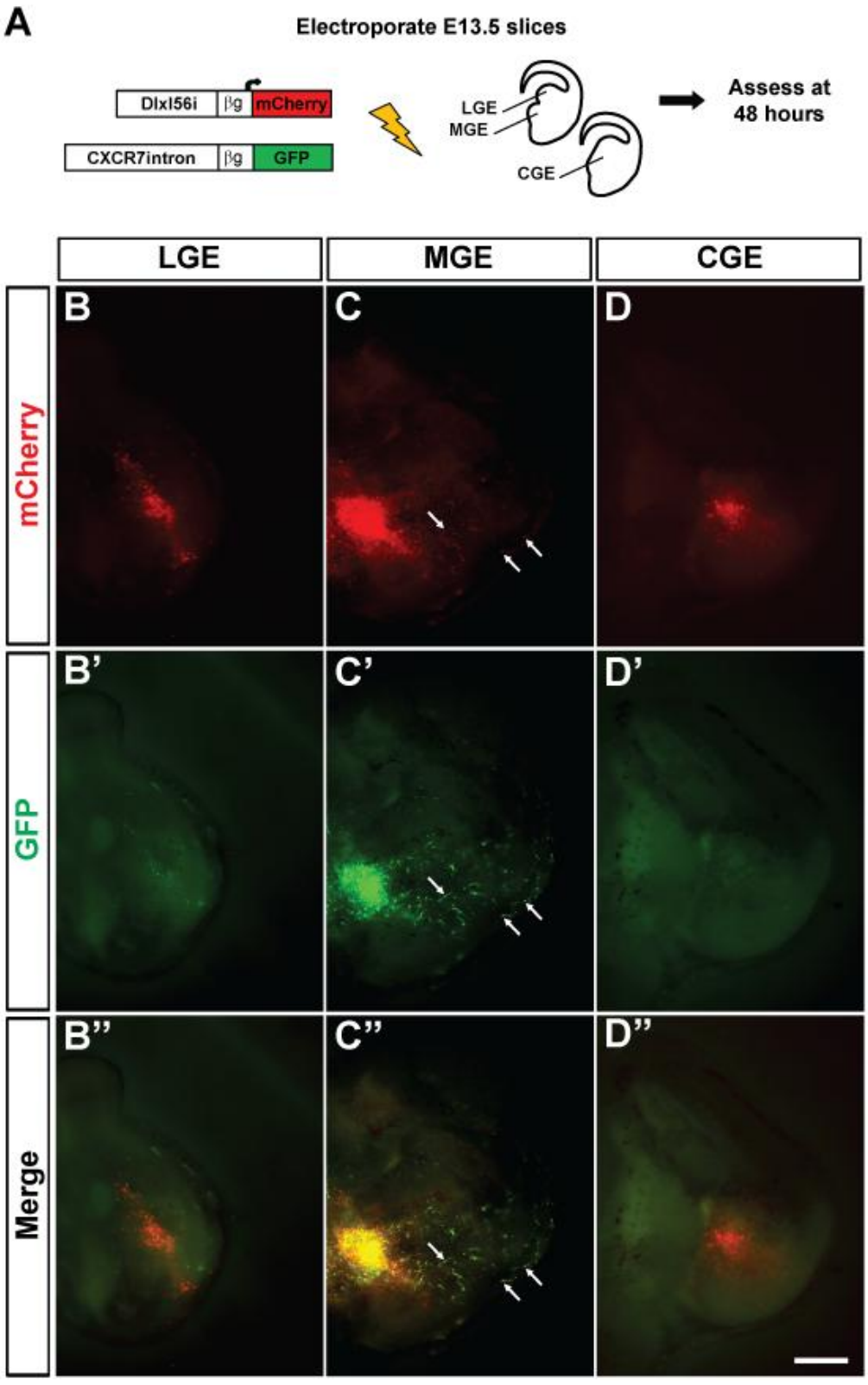
A
Electroporate E13.5 slices
Dlx1I56i
βg
mCherry
CXCR7intron
βg
GFP
LGE
MGE
CGE
Assess at
48 hours
LGE
MGE
CGE
mCherry
GFP
Merge
B
C
D
B'
C'
D'
B''
C''
D''

Table S1

		Intrinsic membrane properties							
		RMP (mV)	R input MΩ	Cm (pF)	Tm (ms)	AP Threshold	AP Amplitude	Spike Adaption	Sag Amplitude
RSNP	WT (n=12)	-57.3 ± 1.8	548.6 ± 102.8	35.9 ± 4.8	41.0 ± 8.8	-40.8 ± 1.7	50.8 ± 5.1	2.6 ± 0.7 ††	1.9 ± 0.6
	Ihx6 ko (n=15)	-56.1 ± 1.8	753.6 ± 130.4	30.0 ± 2.4	33.1 ± 6.9 †	-39.8 ± 1.3	49.2 ± 3.5	2.2 ± 0.3 ††	1.7 ± 0.5
FS	WT (n=4)	-66.8 ± 3.1	166.7 ± 61.2	31.8 ± 3.7	14.8 ± 3.9 †	-41.4 ± 8.1	51.0 ± 5.6	1.7 ± 0.1 ††	1.0 ± 0.4
	Ihx6 ko (n=3)	-66.0 ± 1.5	152.5 ± 19.9	38.0 ± 6.2	18.5 ± 7.3 †	-37.2 ± 0.8	58.9 ± 7.0	1.4 ± 0.3 ††	0.7 ± 0.4
BS	WT (n=2)	-66 .0 ± 8.0	474.6 ± 56.4	48.5 ± 18.5	108.9 ± 72.6	-48.6 ± 4.5	68.6 ± 9.4	11.1 ± 3.7	2.1 ± 0.1
	Ihx6 (n=0)								
LS	WT (n=0)								
	Ihx6 (n=7)	-69.9 ± 2.0	319.2 ± 37.0	32.4 ± 1.5	26.3 ± 8.9 †	-35.6 ± 2.8	49.7 ± 4.8	1.4 ± 0.1 ††	0.7 ± 0.4

		EPSC properties			
		FREQ	AMP	10-90RT	DTC
RSNP	WT (n=12)	5.7 ± 1.3 **	15.1 ± 2.3	1.1 ± 0.04	2.7 ± 0.2
	Ihx6 ko (n=15)	3.5 ± 0.6 **	15.1 ± 2.3	1.09 ± 0.05	2.6 ± 0.2
FS	WT (n=4)	27.3 ± 8.8	15.3 ± 2.9	0.9 ± 0.1	1.6 ± 0.3
	Ihx6 ko (n=3)	14.4 ± 6.5	17.1 ± 1.3	0.9 ± 0.1	1.5 ± 0.3
BS	WT (n=2)	6.9 ± 6.3 *	13.8 ± 2.6	1.0 ± 0.2	1.9 ± 0.3
	Ihx6 (n=0)				
LS	WT (n=0)				
	Ihx6 (n=7)	5.0 ± 0.8 **	9.1 ± 0.2	0.9 ± 0.03	1.8 ± 0.1

*	P < 0.05 versus WT FS
**	P < 0.01 versus WT FS
†	P < 0.05 versus BS
††	P < 0.01 versus BS

Supplemental Figure legends

Supplemental Figure 1: In situ analysis of 5HT3aR, COUPTFII and cMaf in control and *Lhx6*$^{PLAP/PLAP}$ brains shows no major phenotype. Related to Figure 1.

In situ hybridization (ISH) from control and *Lhx6* mutant E15.5 and P14 brains. Coronal hemisections of a rostral (left) to caudal (right) series at E15.5 is shown for 5HT3aR (A), COUPTFII (B) and cMaf (C). Rostral and caudal coronal neocortical regions at P14 for 5HT3aR, COUPTFii and cMaf in controls (D-I), and *Lhx6* mutants (D'-I'). Scale bars: (C) = 1mm; (I') = 500µm.

Supplemental Figure 2: MGE transplantation of *CAG-dsRed* control and *Lhx6*$^{PLAP/PLAP}$. Related to Figure 2.

(A) Schema depicting MGE transplantation of E13.5 control or *Lhx6*$^{PLAP/PLAP}$ expressing dsRed into P1 WT neocortex, and analysis at 25 days post transplant (DPT). (B, C) Immunofluorescent analysis of controls and mutants for NeuN and dsRed in the neocortex at 25 DPT. Arrows point to dsRed^{+} cells that express NeuN. (D) Quantification of cell fate for control and mutant cells for NeuN and the interneuron subtype markers somatostatin (SST) and parvalbumin (PV). (E) Quantification of the proportion of dsRed^{+} transplanted cells that reside in neocortical layer I normalized to all dsRed^{+} cells transplanted. Data expressed as ± SEM, $^{**}p < 0.01$, $^{***}p < 0.001$. Scale bar in (C) = 100 µm.

Supplemental Figure 3: *DlxI12b* enhancer lentiviral vectors and expression assessment. Related to Figures 3, 4 and 5.

(A) Schema depicting lentiviral vectors that utilize the *DlxI12b* enhancer and beta-globin (βg) minimal promoter to drive expression of GFP and a gene of interest separated by the T2a

peptide. (B) Western blot analysis of HEK293T cell lysates that were transfected with the lentiviral DNA vectors. Text to the left denotes the antibodies used and text below denotes which vectors were transfected into the cells. (C-E) Immunofluorescent images of transplanted E13.5 *CAG-dsRed* MGE cells that were first transduced with a *DlxI12b-GFP* virus and assessed at 10 DPT (image is from neocortex). Scale bar in (E) = 250µm.

Supplemental Figure 4: Assessment of ChAT and SOX6 after *Lhx8* transduction of transplanted MGE cells. Related to Figure 4.

(A-D) Immunofluorescent images of E13.5 control MGE cells that were transduced by *GFP* or *Lhx8*, transplanted into P1 neocortices and assessed for ChAT at 35 DPT. (E, F) ChAT staining of striatal tissue from the same sections used in (A-D). (G) Quantification of GFP^+ transduced cells that expressed ChAT in the neocortex at 35 DPT. (H-O) Immunofluorescent images of E13.5 control (H, I, L, M) or Lhx6 mutant (J, K, N, O) MGE cells that were transduced by *GFP* or *Lhx8*, transplanted into P1 neocortices and assessed for SOX6 at 35 DPT. Quantification of GFP^+ transduced cells that express SOX6 for control (P) or *Lhx6* mutant (Q) MGE transplant groups. Arrows point to cells that co-express GFP and SOX6. Scale bar in (O) = 100µm.

Supplemental Figure 5: Arx does not rescue Satb1 expression in *Lhx6* mutants. Related to Figure 4.

Immunofluorescent images of neocortex from P13 controls (A-C) and *Lhx6* mutants (D-F), stained for SATB1/2 and tdTomato. Arrows point to examples of double-positive cells. (G-L) Immunofluorescent images of E13.5 Lhx6 mutant MGE cells that were transduced by *GFP* or *GFP-T2a-Arx* lentiviruses, transplanted into P1 WT neocortices and assessed for SATB1/2 and GFP at 35 DPT. *GFP* and *Arx* transduced *Lhx6* mutant cells show little to no expression of SATB1/2 protein at 35 DPT. Scale bars in (F, L) = 100µm.

Supplemental Figure 6: Transplanted *Lhx6* mutant MGE cells express Sp8. Related to Figure 5.

Immunofluorescent images of E13.5 Lhx6 mutant MGE cells that were transduced by *GFP*, transplanted into P1 WT neocortices and assessed for Sp8 and GFP at 35 DPT. Sp8 expression was present in Lhx6 mutant transplanted MGE cells (arrows) but not in control transplants. Scale bar in (B) = 100µm.

Supplemental Figure 7: Expression of CXCL12-GFP in the postnatal neocortex. Related to Figure 6.

(A-C) Immunofluorescent images of CXCL12-GFP neocortical expression at P5, P10 and P14, (v) = neocortical layer v. Scale bar in (C) = 100 µms.

Supplemental Figure 8: The *CXCR7-intronic* enhancer is expressed in the MGE. Related to Figure 7.

(A) Schema of slice electroporation. E13.5 coronal slices were co-electroporated with *CXCR7intron*-GFP and *DlxI56i*-mCherry vectors. Native mCherry, GFP and merged fluorescent images of slices containing LGE (B,B',B''), MGE (C,C',C'') or CGE (D,D',D'') tissues 48 hours after electroporation. Arrows point to examples of GFP/mCherry colocalized cells. Scale bar in (D'') = 250µm.

Supplemental Table 1: Electrophysiological properties of transplanted MGE cells from control and *Lhx6*$^{PLAP/PLAP}$. Related to Figure 3.

Top table: intrinsic membrane properties recorded from different subgroups of neurons at 35 days after transplantation comparing control and *Lhx6* mutant cells as well as the properties between subgroups. Bottom table: Comparison of average EPSC properties received from either control or *Lhx6* mutant neurons. Abbreviations: (RSNP) regular spiking non-pyramidal,

(FS) fast spiking, (BS) burst spiking, (LS) late spiking, (Rmp) resting membrane potential, (R input) input resistaance, (Cm) whole cell capacitance, (Tm) membrane time constant, (AP) action potential, (RT) rise time, (DCT) decay time constant. OneWay ANOVA with Tukey post test was used to test significance among the groups.

Supplemental experimental procedures

Animals

CAG-dsRed mice were maintained on a CD-1 background and have previously been reported (Vintersten et al., 2004).

Antibodies and reagents

DsRed (Clontech), GFP (Aves), calretinin (Immunostar), parvalbumin (Swant Swiss Abs), somatostatin (Chemicon), VIP (Immunostar), SP8 (SantaCruz), Reelin (Millipore), NeuN (Chemicon), SatB2, cross reacts with Satb1 (abCam), Sox6 (AbCam), CxCR7 (11G8 from R&D systems), M2 anti-Flag (Sigma), Lhx6 (AbCam), Arx (SantaCruz). Alexa-conjugated secondary antibodies were from Molecular Probes. Sections were cover slipped with Vectashield containing DAPI (Vector labs). For western blots, secondary HRP antibodies were from Biorad. We generated the rabbit anti-Lhx6 polyclonal affinity-purified antibody at Genscript using Human Lhx6 amino acids 1-67 (based on Lhx6.1a numbering).

Cell counting

Sections used for all cell counting experiments were coronal and 25 µm thick. For cell density counting from transgenic crosses, 10x images were taken from the somatosensory cortex, encompassing all neocortical layers. All cells in the neocortical fields were counted, and divided by the area of the neocortex to determine cell density. For cell fate markers and lamination assessment counting of transplanted MGE cells, we assessed cells based on the following

criteria: 1) All cells in the neocortex were counted from a serial sectioned brain, as long as the cells were at least 250μms away from the injection site. 2) Transplant experiments with ~50 cells/serial section series (or greater) for each parameter were used. 3) Each parameter was normalized to either GFP or dsRed to calculate the proportion of cells that express a specific marker. 4) For lamination counts, we used DAPI to subdivide neocortical layers and counted all cells in the rostral to caudal serial sections. We did not count any cells at or within 250μm of an injection site nor cells at the midline.

Chromatin immunoprecipitation and qPCR

Basal ganglia were micro-dissected and cross-linked at room temperature for 10 minutes in 1% Formaldehyde. The cross-linked chromatin was sheared using a Bioruptor^{TM} UCD-200 for 15 rounds (1 round = 30s on/1min off at High Intensity). The sheared chromatin was incubated with primary antibody (roughly 4μg) over night at 4°C. 20-fold molar excess of blocking peptide (Lhx6 amino acids 1-67) was added to a negative control as well as a fraction of crude chromatin is saved as input. Protein/antibody complexes were collected using Dynabeads (40μl Protein A + 40μl Protein G, Invitrogen), washed, eluted and reverse cross-linked according to the Millipore-Upstate ChIP protocol. ChIP-qPCR analysis was performed on a 7900HT Fast Real-Time PCR System (Applied Biosystems) using SYBR GreenER qPCR SuperMix (Invitrogen), and qPCR data analyzed as in (Vokes et al., 2007).

The following primers were used for qPCR: Arx enhancer sites (A1: 5' ACCCAAAAGCAATCATGTCATC, 3' ATGTGCTTCTGACAGGCTCC), (A2: 5' ACAGACGCTTCCAATTCCCG, 3' TCCATTAACTTCATCATGCTCACT), (A3: 5'

TATTAGATGTTATCAGGCAGCTGGA, 3' CTCTGCAATTATGCTCGCAC), (A4: 5' TGTGCGAGCATAATTGCAGAGA, 3' TCCAGTTCTCCTCCCTTCCTG), (A5: 5' AGGACAAAAAGAAATAGCAAAACCA, 3' GCCAGCAATTTCAAACACAGT) and CXCR7 enhancer sites (C1: 5' GGTCTGACCCAAGGCACTCAGC, 3' CAGCAACGCCCGCCATGAGA), (C2: 5' GCAAGCTTGACAAACCAACATCGAA, 3' CCGGGAGTTCCTTTGAATGCCTGT), (C3: 5' GGGGTGGGGATGGATTAATTCACAG, 3' AGCAGGGGTGCCATGAAGAGA), (C4: 5' TTGAATGTTAGCTCCTCTTCATC, 3' CCAATTGAAGTTGGACAACAC), (C5: 5' TGTCTCTCCATTCATTTGCTCA, 3' TCTCAGGGATGCCACTAACC), (C6: 5' GGGCTTTGGAGGGGAGTTTATCCA, 3' CCCTTGGCCAGCTCTGGGTC), (C7: 5' TGGGAGTGCTGTCTGTGTGCAG, 3' GCCTCCTCCAGAGGCCGACT), (C8: 5' GCAGTGGCTCATTCCCTCCCC, 3' GCAGCCTCGCCTTCCTCCAG), (C9: 5' GGCTCTCTGGGAGGTCGGCA, 3' TGGACTCCAGTCCTGGACAAAGC), (C10: 5' ACGTCCAGAAGCATCTGCATTTCCA, 3' ACTGTTCAAGGGAAGACACTGACCT).

Electrophysiology

Slice preparation

Mice were deeply anesthetized by katamine/xalyazine administration and decapitated. The brain was removed and immersed in ice-cold (2–4°C) oxygenated high-sucrose artificial cerebral spinal fluid (ACSF) containing the following (in mM): 150 sucrose, 50 NaCl, 25 $NaHCO_3$, 10 dextrose, 2.5 KCl, 1 NaH_2PO_4-H_2O, 0.5 $CaCl_2$, and 7 $MgCl_2$, and equilibrated with 95% O_2–5% CO_2, pH 7.2–7.4, 300–305 mOsm/kg. Brains were blocked, glued to a sectioning stage, and 300-µm-thick coronal slices were cut in ice-cold, oxygenated high-sucrose ACSF using a Vibratome (Leica VTS1000). Slices were then transferred to a storage chamber containing oxygenated ACSF containing the following (in mM): 124 NaCl, 3 KCl, 1.25 NaH_2PO_4-H_2O, 2

$MgSO_4$-$7H_2O$, 26 $NaHCO_3$, 10 dextrose, and 2 $CaCl_2$ (pH 7.2–7.4, 300–305 mOsm/kg), heated at 35°C for ~45 minutes in a water bath, and maintained at room temperature until use for experimentation.

Electrophysiology

After an equilibration period of at least 60 min, slices were transferred to a recording chamber on an upright, fixed-stage microscope equipped with infrared, differential interference contrast (IR-DIC) and epifluorescence optics to visualize GFP-labeled cells (Olympus BX50WI), where they were continuously perfused with warmed (34-35°C) ACSF. Patch pipettes were pulled from borosilicate glass (1.5 mm outer diameter and 0.45 mm wall thickness; World Precision Instruments) with a P-87 puller (Sutter Instrument). Open tip resistance was 3–5 MΩ. The intracellular solution contained the following (in mM): 140 K^+ gluconate, 1 NaCl, 5 EGTA, 10 HEPES, 1 $MgCl_2$, 1 $CaCl_2$, 3 KOH, 2 ATP, and 0.2% biocytin, pH 7.21. Recordings were obtained with an Axopatch 1D amplifier (Molecular Devices), filtered at 5 kHz, and recorded to pClamp 10.2 (Clampfit; Molecular Devices). After membrane rupture, cells were first voltage clamped for ~5 min at −70 mV (i.e., near resting membrane potential) to allow equilibration of intracellular and recording pipette contents. Resting membrane potentials were measured immediately after breakthrough by temporarily removing the voltage clamp and monitoring voltage. Series resistance was typically <15 MΩ and was monitored throughout the recordings. Data were only used for analysis if the series resistance remained <20 MΩ and changed by ≤20% during the recordings. Recordings were not corrected for a liquid junction potential. For voltage-clamp recordings, a 2-5 min sample recording per cell was used for measuring spontaneous excitatory postsynaptic current (sEPSC) frequency, amplitude, 10-90% rise time, and decay time constant at a holding potential of −70 mV. Events characterized by a typical fast rising phase and exponential decay phase were manually detected using MiniAnalysis (Synaptosoft). The threshold for event detection was currents with amplitudes greater than three

times the root mean square (RMS) noise level. For current-clamp recordings, cells were held at -70 mV, and intrinsic electrophysiological properties were measured in response to a series of long (1000 ms) hyperpolarizing and depolarizing current-injections (10 pA steps; range: -50 pA to 1000 pA). Input resistance (R_{input}) was measured from peak voltage responses to ±10 pA current injections (1000 ms duration). Membrane time constant (τ_m) was calculated by fitting the voltage response to a -10pA hyperpolarizing current pulse with a single exponential function ($y = y_0 + Ae^{-t/\tau_m}$, where y_0 is the y asymptote, A is amplitude, τ_m is decay time constant, and t is time). Spike accommodation was identified by examining the ratio of the interspike intervals between the last two action potentials in the train as compared to the first two at 2x spike threshold.

In situ hybridization

Coronal cryostat sections were prepared and processed as described in (Jeong et al., 2008). Briefly, either E15.5 or P14 were fixed in 4%PFA then sunk in 30% sucrose before cutting 20 µm sections. The following probes were used on E15.5 and P14 coronal serial sections from control and $Lhx6^{PLAP/PLAP}$ brains. COUPTFii (M. Tsai), 5HT3aR (B. Rudy), cMaf (McKinsey et al., 2013).

MGE slice electroporation

E13.5 brains were dissected in ice cold HBSS then embedded in 4% low-melting agarose in PBS. Next, 250µm coronal sections were made with a VT1200S vibratome (Leica). Live sections were placed atop a permeable nucleopore Track-Etch membrane (Whatman) floating in DMEM H21 + 10% FBS. Following a two hour recovery at 37ºC , slices were injected with a

DNA mixture containing CXCR7intron-GFP and DlxI56i-mCherry vectors (at a 3:1 molar ratio). Injected slices were electroporated with a BTX ECM830 electroporator equipped with two platinum electrodes; one fixed to a glass petri dish and one that is lowered onto the slice. 1% Agarose in PBS was used as the conductive surface between the electrodes and the slice. Each Slice was given three 5ms pulses at 100V. After Electroporation, the DMEM H21 + 10% FBS was replaced with serum free growth media (Neurobasal supplemented with B27, 0.5% Glucose, 1X Glutamine, 1X Penicillin-Streptomycin) and slices were cultured at 37ºC for 48 hours before assessing fluorescence activity.

MGE transplantation and transduction

E13.5 MGEs from individual embryos were dissected in ice-cold HBSS and then kept on ice in DMEM media (containing 10% fetal bovine serum). MGEs were then mechanically dissociated with a p1000 pipette tip and then either concentrated for injections or infected with lentiviruses. For lentiviral infections, dissociated MGE cells were mixed with pre-warmed media, polybrene (8 µg/ml), and about 10-20 uls of concentrated lentiviruses, and incubated at 37°C for 30 minutes, with agitation. Cells were then pelletted in a tabletop centrifuge at low speed (500xg, 3 minutes) and washed with 2-3 times with media followed by trituration to disperse cells between each wash to remove excess virus. A final cell pellet was resuspended in 2-3 ul of media, put on ice, and then remaining media was removed before loaded into the injection needle. For injections, a glass micropipette of 50 µm diameter (with a beveled tip) was preloaded with sterile mineral oil and cells were front-loaded into the tip of the needle using a plunger connected to a hydraulic drive (Narishige) that was mounted to a stereotaxic frame. Pups were anesthetized on ice for 1-2 minutes before being placed on the mold for injections. Each pup received ~3 injections of cells (~ 70 nl per site), in the right hemisphere. These sites were about 1 mm apart from rostral

to caudal and were injected into layers V-VI of the neocortex. After injections, pups were put back with the mother to recover. Mice were sacrificed between 10-35 days (depending on the assay) after transplant and transcardially perfused with PBS followed by 4% PFA. Brains were then postfixed in 4% PFA and sunk in 30% sucrose before embedding in OCT. Embedded brains were sectioned by cryostat to generate coronal serial sections of 25 µm thickness at intervals of 250 µm from rostral to caudal.

Vector generation

Reporter and transcription factor expression vectors:

The CXCR7 intron was PCR amplified (5' GAGAGGTACCCAGCTGGATACCGCAGGCAG, 3' GAGACTCGAGCCACCTCAGCCTGACCTTCA) from mouse genomic DNA (Roche), and ligated into 5' KpnI and 3' XhoI sites of the PGL4.23-luciferase (Promega). The pCAGGs-Ldb1 and CMV-Lhx6-IRES-GFP expression vectors were previously described (Flandin et al., 2011). The PGL4.23 luciferase vector was previously modified to replace the luciferase gene with a beta-globin minimal promoter and mCherry reporter (Flandin et al., 2011). To replace mCherry with GFP, a beta-globin-GFP fragment was digested from the DlxI12b-GFP lentiviral vector with 5' XmaI (cuts internal to beta-globin minimal promoter) and 3' BsrGI sites and ligated into the same sites of the PGL4.23 vector. The CXCR7-intron was then ligated into 5' KpnI and 3' XhoI sites upstream of the beta globin and GFP. The DlxI56i-beta-globin-mCherry reporter was made by replacing the luciferase gene from a PGL4.23 DlxI56i-luciferase vector with mCherry as described in (Flandin et al., 2011).

DlxI12b-GFP-T2a-mcs lentiviral vectors:

The mouse DlxI12b and beta-globin minimal promoter were amplified as a single unit by PCR (primers: 5' GAGAGGATCCACACAGCTTAATGATTATC, 3' GAGAACCGGTCGCCGCGCTCTGCTTCTGG) from a DlxI12b-beta-globin-Cre vector (Potter et al., 2009) with introduced 5’ BamHI and 3’ AgeI sites. A CMV-GFP-T2a-mcs vector was digested with BamHI and AgeI to remove a CAG enhancer and CMV promoter 5' to the GFP gene, and the DlxI12b-beta-globin was ligated in this spot. Human Lhx6, human CXCR7, and mouse Arx were PCR amplified with introduced SphI sites (Lhx6: 5' GAGAGCATGCATGGCCCAGCCAGGGTCC, 3' GAGAGCATGCGTACTGAAAAAGGATGAC; CXCR7: 5' GAGAGCATGCATGGATCTGCATCTCTTC, 3' GAGAGCATGCTCATTTGGTGCTCTGCTC; Arx: 5' GAGAGCATGCATGAGCAATCAGTACCAGG, 3' GAGAGCATGCTTAGCACACCTCCTTCCC; CXCR7: 5' GAGAGCATGCATGGATCTGCATCTCTTC, 3' GAGAGCATGCTCATTTGGTGCTCTGCTCC) and cloned in frame, 3’ to the T2a sequence of DlxI12b-GFP-T2a-mcs. human Sox6 and 3x-Flag-(human)-Lhx8 were first PCR amplified with (Sox6: 5' CCAAGAATTCATGTCTTCCAAGCAAGCC, 3' GAGACCCGGGTCAGTTGGCACTGACAGCC; 3xFlag-Lhx8: 5' GAGAGAATTCTCAGAATTAACCATGGAC, 3' GAGACCCGGGTTAGGTATGACTTATTGGC) and cloned into the EcoRI and XmaI of the CMV-GFP-T2a-mcs vector. Next, the CAG-CMV was cut out and the DlxI12b-beta-globin minimal promoter ligated into these vectors as described above.

CXCR7intron-GFP-T2a-Cre:

Cre was PCR amplified (5' GAGAGCATGCATGTCCAATTTACTGACC, 3' GAGACCATGGTCACACCGGTCCATCGCC) with 5' SphI and 3' NcoI sites and introduced in frame 3' to the T2a in the *DlxI12b-GFP-T2a-mcs* vector. Next, DlxI12b was removed from the

resulting vector with XbaI and EcoRI and the mouse CXCR7intron was PCR amplified (5' GAGATCTAGACAGCTGGATACCGCAGGCAG, 3' beta-globin described above), digested with XbaI and XmaI and ligated to the vector containing Cre to generate the final vector. All vectors were verified by sequencing.

Western blots

HEK293T cells, grown in DMEM with 10% fetal bovine serum, were transfected with the lentiviral vectors using Fugene6. Cell lysates were harvested at 48 hours post transfection with either RIPA buffer (25mM Tris-HCl pH 7.6, 150 mM NaCl, 1% NP40, 0.1% SDS. 1% sodium deoxycholate) to harvest total cell lysates or with a nuclear isolation kit (Pierce), to collect nuclear fractions. 20 µg of cell lysates were separated on SDS-PAGE gels, transferred to nitro-cellulose membranes and then probed with specific antibodies before detection by chemiluminescence.

Supplemental references

Zerucha, T., Stuhmer, T., Hatch, G., Park, B.K., Long, Q., Yu, G., Gambarotta, A., Schultz, J.R., Rubenstein, J.L., Ekker, M. (2000). A highly conserved enhancer in the Dlx5/Dlx6 intergenic region is the site of cross-regulatory interactions between Dlx genes in the embryonic forebrain. Journal of Neuroscience *20*, 709-21.